AN INSTRUMENT FOR RECORDING AND ANALYSIS OF HEART SOUNDS

by

Gözde Güvendi

B.S., Electrical and Electronics Engineering, Yeditepe University, 2018

Submitted to the Institute for Graduate Studies in
Science and Engineering in partial fulfillment of
the requirements for the degree of
Master of Science

Graduate Program in Electrical and Electronics Engineering
Boğaziçi University

2022

ACKNOWLEDGEMENTS

First of all, I would like to thank my master thesis advisor, Prof. Dr. Yasemin Kahya, for giving me the opportunity to work with her and other valuable professors, as well as for leading me with her vast knowledge and supporting me to improve my work. I am also very pleased that she gave me the opportunity to work at Boğaziçi University Lung Acoustic Laboratory (LAL).

I would like to thank Asst. Prof. İpek Şen and Lecturer Kemal Ozanoğlu, and LAL members who shared their valuable information with me and supported my work at the meetings I attended during my master thesis. At the same time, I am grateful to Prof. Dr. Oğuzhan Çiçekoğlu, who accepted to participate in my thesis committee and will evaluate my work with his valuable comments.

I would like to express my endless gratitude to my esteemed family, who have never ceased to support me during this process. It was not possible for me to achieve these successes without my family, who had great efforts on me. Thanks to them, I have been able to go through a difficult process easier, so I feel very lucky to have them.

Finally, I would like to express my endless gratitude to my valuable friends and colleagues, especially Oğulcan Burak Boz for their contributions to my master thesis and for their moral support. I would also like to express my gratitude to Yeditepe University RF Laboratory, which provided me with material support for my thesis.

ABSTRACT

AN INSTRUMENT FOR RECORDING AND ANALYSIS OF HEART SOUNDS

According to the data of the WHO, heart diseases are the leading diseases with high level mortality rates. In 2019, 17.9 million individuals died due to CVDs, this number is constituting 32 percent of the death rates. For this reason, early diagnosis of heart diseases still maintains its significance today.

While the diagnosis of these diseases is made by traditional auscultation methods, advanced technological digital stethoscopes are also used in today's technology. Thanks to these devices, the auscultated sound can be interpreted automatically, at the same time recorded and listened to again later, and cardiac dysfunction can be detected with advanced classification algorithms. Thus, these systems may prevent misinterpretations and create a crucial benefit for early diagnosis. This thesis aims to develop a portable heart sound acquisition, recording and automatic analysis device. The purpose is to design a system which has a long life with low cost and low power consumption. Proposed instrument enables recording of the amplified and filtered sound with a user-friendly interface. At the same time, heart sounds can be listened to directly on the device at the desired volume level with the headphone output thanks to this instrument.

The analog data converted to digital is transmitted to both the mobile phone and the computer using Bluetooth Low Energy technology, and the signal can be monitored and analyzed on computer based GUI. User friendly interface shows people's heart rate and heart rate variability value. In this way, users can have information about their stress levels and heart related issues.

ÖZET

KALP SESLERİ KAYIT VE ANALİZ CİHAZI

Dünya Sağlık Örgütü'nün verilerine göre kalp hastalıkları ölüm oranlarının yüksek olduğu hastalıkların başında gelmektedir. 2019 yılında kalp hastalıkları nedeniyle 17,9 milyon kişi hayatını kaybetti, bu sayı ölüm oranlarının yüzde 32'sini oluşturuyor. Bu nedenle kalp hastalıklarının erken teşhisi günümüzde hala önemini korumaktadır.

Bu hastalıkların teşhisi geleneksel oskültasyon yöntemleri ile yapılırken günümüz teknolojisinde ileri teknolojik dijital stetoskoplar da kullanılmaktadır. Bu cihazlar sayesinde duyulan ses otomatik olarak yorumlanabilmekte, aynı anda kaydedilip daha sonra tekrar dinlenebilmekte ve gelişmiş sınıflandırma algoritmaları ile kalp fonksiyon bozuklukları tespit edilebilmektedir. Böylece bu sistemler gerçekleşebilecek yanlış yorumlamaları önleyecek ve teşhis için çok önemli bir fayda sağlayacaktır. Bu tez, taşınabilir bir kalp sesi toplama, kayıt ve analiz cihazı geliştirmeyi amaçlamaktadır. Amaç, düşük maliyetli ve düşük güç tüketimi ile uzun ömürlü bir sistem tasarlamaktır. Önerilen enstrüman, kullanımı kolay bir arayüzde, güçlendirilmiş ve filtrelenmiş sesi kaydetmeyi mümkün kılmaktadır. Aynı zamanda bu cihaz sayesinde kulaklık çıkışı ile kalp sesleri doğrudan cihaz üzerinde istenilen seviyede dinlenebilmektedir.

Dijitale dönüştürülen analog veriler Bluetooth Low Energy teknolojisi kullanılarak hem cep telefonuna hem de bilgisayara iletilir ve sinyal, bilgisayar tabanlı GUI üzerinden izlenebilir ve analiz edilebilir. Kullanıcı dostu arayüz, insanların kalp atış hızı ve kalp atış hızı değişkenlik değerini gösterir. Bu sayede kullanıcılar stres düzeyleri ve kalp ile ilgili sorunları hakkında bilgi sahibi olabilirler.

TABLE OF CONTENTS

LIST OF FIGURES

LIST OF TABLES

LIST OF SYMBOLS

Ω	Ohm
π	Pi
ω	Angular Frequency
#	Number

LIST OF ACRONYMS/ABBREVIATIONS

3D	Three Dimensional
A	Ampere
ABN	Abnormal
AC	Alternating Current
ADC	Analog to Digital Converter
AR	Aortic Regurgitation
AS	Aortic Stenosis
ASCII	American Standard Code for Information Interchange
BLE	Bluetooth Low Energy
bpm	Beat per Minute
C	Capacitance
cm	Centimeter
CVDs	Cardiovascular Diseases
DAC	Digital to Analog Converter
dB	Decibel
dBm	Decibel-Milliwatts
DC	Direct Current
DK	Development Kit
ECG	Electrocardiogram
f	Frequency
fA	Femtoampere
FDM	Full Deposition Modeling
FFT	Fast Fourier Transform
fH	High Cut-off Frequency
fL	Low Cut-off Frequency
GND	Ground
GUI	Graphical User Interface
HOCM	Hypertrophic cardiomyopathy

HR	Heart Rate
HRV	Heart Rate Variability
HS	Heart Sound
Hz	Hertz
IC	Integrated Circuit
IMFs	Intrinsic Mode Functions
IoT	Internet of Things
kΩ	Kiloohm
kB	Kilobyte
kHz	Kilohertz
LAL	Lung Acoustics Laboratory
LED	Light Emitting Diode
LTV	Long-term Heart Rate Variability
mA	Milliampere
max	Maximum
Mbps	Megabits per Second
MCU	Microcontroller Unit
mm	Millimeter
MR	Mitral Regurgitation
MRI	Magnetic Resonance Imaging
ms	Millisecond
MS	Mitral Stenosis
mV	Millivolt
MVP	Mitral Valve Prolapse
mW	Milliwatt
N	Normal
nF	Nanofarad
PCB	Printed Circuit Board
PCG	Phonocardiogram
PDA	Patent Ductus Arteriosus
pF	Picofarad

PLA	Polyactic Acid
PR	Pulmonary Regurgitation
PS	Pulmonary Stenosis
PVC	Polyvinyl Chloride
Q	Charge
R	Resistance
RAM	Random-Access Memory
RMS	Root Mean Square
RF	Radio Frequency
S1	First Heart Sound
S2	Second Heart Sound
S3	Third Heart Sound
S4	Fourth Heart Sound
SAADC	Successive Approximation Analog to Digital Converter
SAR	Successive Approximation Register
STV	Short-term Heart Rate Variability
t	Time
TR	Tricuspid Regurgitation
TS	Turner Syndrome
u	Micro
USB	Universal Serial Bus
V	Voltage
Vin	Input Voltage
Vout	Output Voltage
VSD	Ventricular Septal Defect
WHO	World Health Organization

1. INTRODUCTION

1.1. The Literature Review

Cardiovascular diseases (CVD), being very deadly, remain as one of the most important disease group in the medical world. In 2019, approximately 17.9 million people died due to CVD [1]. The diagnosis of these diseases is made by specialist physicians using advanced technological devices or traditional auscultation methods. Mortality rates, which can be reduced with early diagnosis, are based on the experience of the doctors making the diagnosis. Misinterpretation and misdiagnosis can cause death, so advanced diagnostic devices should be used to reduce mortality rates. The high cost of these devices make them inaccessible, so there is an increased need for low-cost and high-accuracy analysis systems that can be used at home. Low-cost and portable devices such as digital stethoscopes have an important place in the diagnosis of cardiac dysfunction. Today, digital stethoscopes are still being developed to make it easier for people to access and to provide accurate disease diagnostic results [2, 3].

1.1.1. Heart Sound Characteristics

The phonocardiogram signals obtained by heart sounds which are generated by acoustic vibrations of heart valves and vessels are divided into 4 segments. These are S1 sounds with a frequency range of 50-150 Hz seen in healthy individuals, systolic pause between S1 and S2 sounds, S2 sounds with a frequency range of 50-200 Hz seen in healthy individuals, and diastolic pause which is seen after S2 sound and before the next S1 sound. The S3 sound in the 50 - 90 Hz frequency range is an abnormal heart sound, which is an indication that people over the age of 40 may have heart diseases; similarly, the S4 sound in the 50-80 Hz range is classified as an abnormal heart sound. The other abnormal sound in the heart is murmur at 200-600 Hz. Table 1.1 shows that measured average duration, frequency and amplitude characteristics of the heart sounds in [4].

In cases where there is a pathological condition in the person, it suppresses the major heart sounds, s1 and s2, as higher frequency murmur sounds begin to dominate. This condition makes it difficult for the healthcare professional to distinguish these complex vocal components and to recognize pitches [2].

Table 1.1. Heart Sound Characteristics.

Sound	**Duration(ms)**	**Frequency(Hz)**	**N/ABN**	**Pitch**
S1	70 -150	50-150	N	High-Pitched
S2	60 -120	50-200	N	High-Pitched
S3	40 -100	50-90	ABN after age of 40	Low-Pitched
S4	40 - 80	50-80	ABN	Low-Pitched

The data collected in the study [4] shows that the the duration an average heart cycle is 800 ms. Approximately 300 milliseconds of this period is allocated as systole time and 500 milliseconds as diastole time. These times are not constant for each cycle and they might vary. Figure 1.1 illustrates the phonocardiogram(PCG) signal which includes heart cycle segments [4].

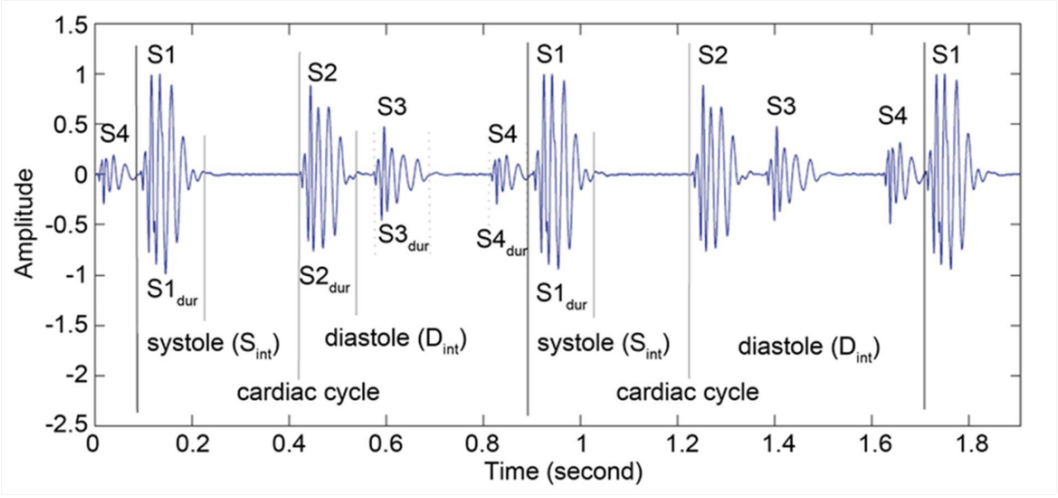

Figure 1.1. Heart Sound Signal [4].

1.1.2. Heart Diseases and Diagnostic Methods

Heart diseases are caused by the heart's inability to perform its working functions properly. The main reasons are overweight, unhealthy and sedentary lifestyle, genetic disorders and use of tobacco products. The diagnosis of some of these diseases is made by heart sound auscultation. One of these disorders is mitral regurgitation. It is a disease that occurs when the mitral valve, located on the left of the heart, does not close properly, and there is leakage from it. On the other hand, mitral stenosis disorder occurs when this valve cannot be opened completely and prevents blood flow. Ventricular septal defect, which is one of the most frequent heart diseases from birth, occurs when there is a hole on the wall separating the heart's left and right ventricles [5] . Hypertrophic cardiomyopathy is a disease that causes difficulty in filling and evacuating blood from the heart due to the thickening of the heart muscles. The blood pumped from the heart flows into the aorta, if there is aortic stenosis, this valve cannot be opened fully and prevents blood flow. This disease is called aortic stenosis. On the contrary, if the valve cannot close completely, this disease is called aortic regurgitation. The units that control the flow of blood between the heart chambers are the tricuspid valves [6]. If the person has tricuspid regurgitation, these valves do not close completely and blood flows back from the lower right chamber to the upper right chamber. In the case of stenosis of these valves, blood that comes from the right atrium cannot flow to the right ventricle. During the diastole period, if blood flows from the pulmonary artery to the chamber which is in the lower right of the heart, it indicates that the person has pulmonary regurgitation. On the other hand, during pulmonary narrowing, insufficient blood flow is provided to the lungs. Another disease is Barlow syndrome which occurs when the mitral valve cannot close normally. Arrhythmia, which is caused by the disruption of the rhythmic electrical conduction of the heartbeat, is another heart disease. Finally, hypertension, which is a very common disease, is a disorder caused by high blood pressure in the vessels [5–7]. In Figure 1.2, the diseases associated with heart sounds and auscultation locations for these sounds are depicted. Also, this figure shows in which cardiac cycle the sounds associated with these diseases can be heard [8].

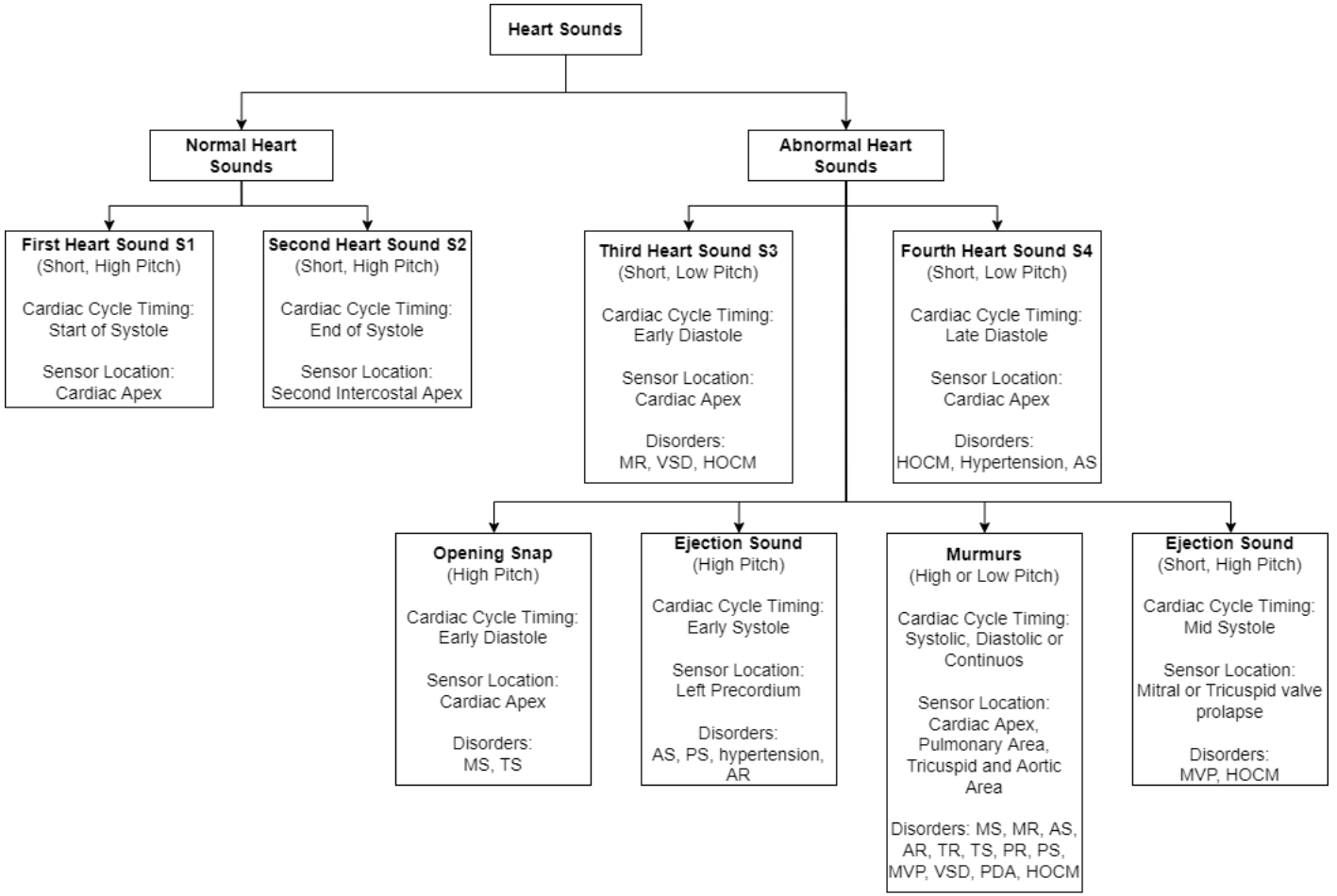

Figure 1.2. Heart Sound Classification and Heart Diseases.

All of these disorders can be detected by using medical diagnostic devices and a variety of methods. MRI, echocardiogram, computed tomography and auscultation are widely used methods. MRI is a 3D imaging technology that has a complex system design. It detects anomalies in the heart structure by the change in the angular movement of protons in the fluid in which the tissue is located. Another diagnostic device is the echocardiogram. This device sends high-frequency sound waves to the body and interprets these sound waves that reflect and create echoes which are transformed into an image from the body, allowing the diagnosis to be made. On the other hand, computed tomography sends x-rays to the human body, creating signals that can be interpreted by the computer to produce body cross-section images. In this way, it enables the detection of dysfunctions. Because these diagnostic methods involve complex system designs, their cost is high and a qualified healthcare professional is needed to use them [8]. On the other hand, it may be sufficient to use an acoustic stethoscope for heart auscultation, which is one of the traditional diagnostic methods, but the correct interpretation of the sound depends on the experience of the doctors.

1.1.3. Auscultation

Cardiac auscultation, where competent healthcare professionals need to use their auscultation and interpretation skills correctly, is listening to the heart with acoustic stethoscopes. Accurate perception of time intervals and pitches in the sound is of great importance in this process, so it is a process that may cause misinterpretations by inexperienced healthcare professionals. The heart sound is obtained using the diaphragm and bell of the acoustic stethoscope, the bell is used to detect low-pitched sounds, while the diaphragm makes it easier to hear high-pitched sounds. The first stethoscope was invented in 1816 by Rene Laennec at the Necker Enfants Hospital in France. This stethoscope is single-channel and made of a wooden tube which can be seen in Figure 1.3. The binaural version of this stethoscope was invented in Ireland in 1851 by Arthur Leard [9, 10].

Figure 1.3. First Stethoscope [9].

Electrical activity in the heart causes the heart to contract. After these contractions, mechanical movements of the atria and ventricles begin. Thanks to this mechanical movement, the valves that open and close provide blood flow. This operation of the heart creates vibrations on the chest piece. The vibrations that occur in the chest during the heartbeat are received by the diaphragm in the stethoscope head and proceed in the tube part of the stethoscope until they reach the earpiece. Reflections occur in this tube due to the collisions of the sound wave, so the sound is transmitted along the tube until it reaches the ear. The points where these vibrations can best be received are the four regions of the chest wall. These are the mitral, tricuspid, pulmonic, and aortic area. Heart sounds are best taken from the mitral area [11]. Auscultation areas can be seen in Figure 1.4.

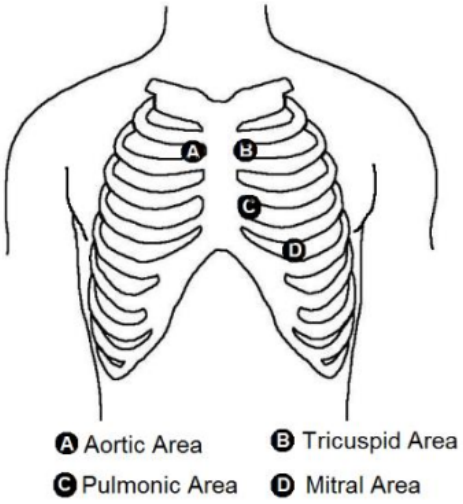

Figure 1.4. Heart Auscultation Areas [11].

1.2. The Aim of the Thesis

The purpose of the thesis is to produce a device that can record and analyze of heart sounds and to design a MATLAB application to process the phonocardiogram signal for disease diagnosis. This low-cost, low energy consuming and portable device enables individuals and health care professionals to listen to filtered heart sound and measure the heart rate and heart rate variability values. In this thesis, first of all, in order to ensure that the sound is transmitted to the electret microphone in the best way, the parts of the acoustic stethoscope are separated and combined with the electret microphone. Additionally, the sound is collected with the capsule head produced in Lung Acoustics Laboratory (LAL) of Boğaziçi University under the leadership of Prof. Dr. Yasemin Palanduz Kahya. At the same time, the vibrations received from the body were converted into an electrical signal with the piezoelectric film sensor and its usage was observed. The vibration, which is formed as a result of the movement of the heart valves and collected from the chest wall, is converted into an electrical signal with the electret microphone. The obtained electrical signal is first amplified and then filtered in accordance with the heart sound frequency range so that it can be processed and listened to at the same time at the later stages. Component preferences used in the designed circuit have been chosen considering features such as affordable

price, low noise and offset production. The obtained filtered signal is adapted to the headphone output with a power amplifier so that the sensor user can listen at the desired volume level. The obtained analog signal was converted into a digital signal with the analog-to-digital converter of the microprocessor and this digital signal was transferred to the computer with the Bluetooth Low Energy (BLE) development kit. The transmitted signal, using the designed MATLAB application, is processed, normalized, segmented and its features are extracted and can be observed via a user-friendly application design. From these features, the person's heart rate and heart rate variability data are calculated and displayed to the user through the interface. At the same time, the system has been optimized for disease detection classification. On the other hand, the resulting sound can be listened to by the user through the application.

1.3. Thesis Outline

This thesis is divided into 8 main headings. In the introduction part, the characteristics of the heart sound, heart diseases that can be detected with digital stethoscope systems and heart auscultation are explained. In the second chapter, data acquisition methods are explained. In this section, the effects of the parts of the acoustic stethoscope on data collection with the digital stethoscope are examined and the structure of the piezoelectric film sensor is presented. In the 3rd chapter, the hardware design is explained. In this section, the subsystems of the sensor are examined and each phase is explained in detail. In addition, the circuit design which contains microphone bias, dc shifter, amplifier, 4th order Bessel filter, power amplifier and regulator design, component selections, simulation results, schematics, and printed circuit board drawings are presented in this section. Part 4 includes embedded system architecture. In this section, information is given about the process of converting the signal from analog to digital, the process of transferring it to a computer with Bluetooth Low Energy(BLE) technology, and power consumption. In chapter 5, software design processes are explained. Processing of the transferred digital data, normalization of the signal, segmentation and feature extraction are explained. The application interface, calculated heart rate and heart rate variability values are shown. In chapter 6, the

mechanical design and internal connections of the system are given. In the 7th chapter, the data and results obtained as a result of the thesis study are shown. The last chapter includes the conclusions. In Figure 1.5, the whole organization of the thesis can be seen.

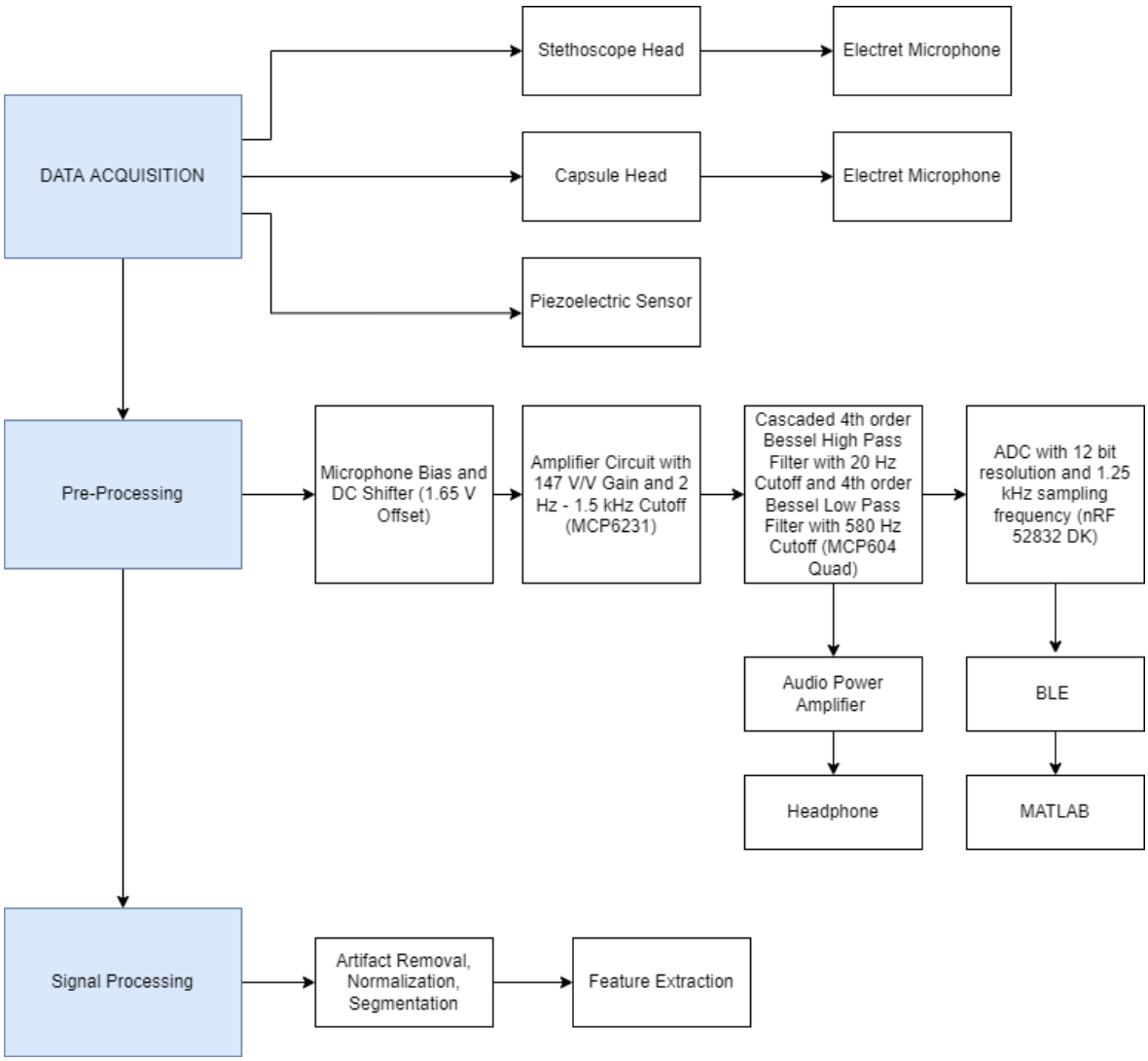

Figure 1.5. Block Diagram of the Heart Sound Recording and Analysis System.

2. HEART SOUND ACQUISITION

2.1. Acoustic Stethoscope

Modern acoustic stethoscopes consist of parts that ensure that the sound is transmitted and heard in the best way. The main parts of the acoustic stethoscope are the headset, tubing and chest piece. The headset includes eartube and eartips and chest piece consist of diaphragm, bell and stem parts. Each of the aforementioned parts has benefits in terms of collecting and transmitting sound properly [12, 13]. These parts are demonstrated in Figure 2.1.

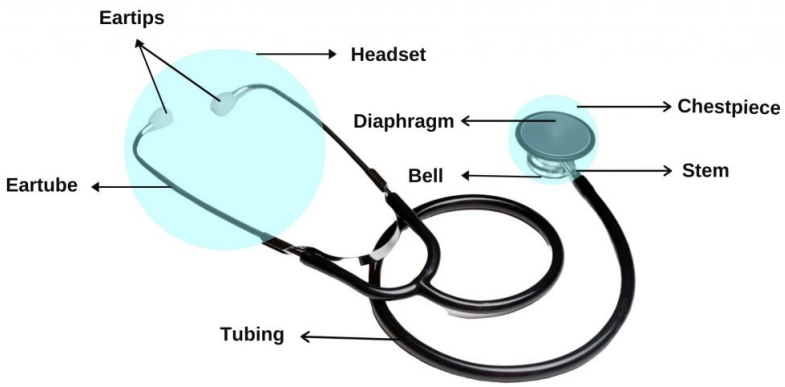

Figure 2.1. Acoustic Stethoscope Parts [12].

The acoustic stethoscope's ear tips are made of silicone or rubber, designed to transmit sound directly from the diaphragm to the ear. Also, ear tips have a seal structure that allows them to fit inside the ear to preclude undesirable sounds. Likewise, specially designed ear tubes are made of metal or steel material to prevent sound loss. It is also the part that connects the diaphragm to the ear tips with a PVC tube. Another main part of the stethoscope, the flexible tube part, connects the diaphragm to the steel ear tubes. There are models used as double or single pipes. The stem, which is made of the same material as the ear tube, is the part that allows the stethoscope user to switch between the diaphragm and the bell. This part is the part that fixes the

chest-piece to the flexible tube. The diaphragm and bell form the circular head of the stethoscope. The diaphragm is used to select high-frequency sounds coming from the body, and a bell is used to listen to the narrowband and lower-frequency sounds [12]. In this thesis, the parts of the acoustic stethoscope are examined separately and their effects are observed. POM-5242L-R electret microphone is used as a transducer by attaching it to an acoustic stethoscope [14].

2.2. Microphone Capsule

One of the most critical points in the signal acquisition process is the contact of the microphone with the skin. Previously, air-coupled microphones and contact microphones were used to collect various audio signals. Ventilation openings, which are not mentioned much in such systems, are to prevent the chamber where the microphone is placed from being under pressure. These vents are important, so as to not impair the frequency response and sensitivity of the microphone. Therefore, ventilation holes are used to allow the pressure inside the chamber to leak out. On the other hand, while they allow the pressure fluctuations to leak out, they reduce the microphone's low frequency sensitivity and allow ambient noise to be transmitted to the microphone.

In order to avoid these problems, the ventilation holes in the system are designed narrowly and acts as an inductive component. This way, sound can be transmitted to the microphone, while ambient noise is kept out and at the same time pressure fluctuations are allowed to leak out. In addition to these, the surface area and diameter of this capsule in contact with the body should be designed to collect the sound in the best way [15]. Considering these important parameters, the microphone capsule designed in Bogazici University Lung Acoustics Laboratory has been produced to transmit the sound to the microphone in the best possible way. The sound collected by the diaphragm will also be picked up by placing the POM-5242L-R electret microphone inside the capsule head. In Figure 2.2, a microphone capsule can be seen.

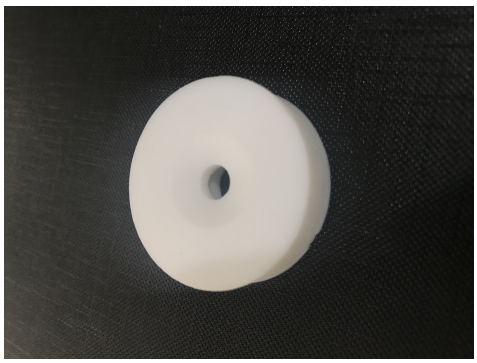

Figure 2.2. Microphone Capsule.

2.3. Piezoelectric Sensor

Condenser microphones are generally used as transducers to convert the heart sound obtained in all the data collection methods mentioned above into electrical signals. In addition, piezoelectric sensors can be used as transducers in heart sound analysis systems [8]. When an external force is applied to the piezoelectric material, the crystal structure and symmetry of the material are disrupted. Mechanical stress from this external force creates a dipole moment and causes an electric field to be generated on the piezoelectric material. Thus, when mechanical stress is applied to the piezoelectric sensor, it starts to generate a charge. In case the piezoelectric transducer is connected to a circuit, the charge on it will not be immobile. For this reason, the time-varying amount of charge can be modeled as a current source. The generated charge is transferred to the circuit with the two electrodes between which the piezoelectric layer is located. These electrodes can be modeled as a capacitor [16]. This piezoelectric sensor can be modeled as in Figure 2.3.

The V_{OUT} expression in Figure 2.3 can be written as

$$\mathbf{V}_{OUT} = \frac{1}{C}\int I dt = \frac{1}{C}\int \frac{dQ}{dt} dt = \frac{Q}{C}\,. \tag{2.1}$$

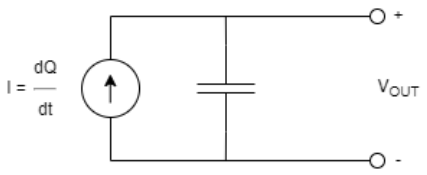

Figure 2.3. The Model of the Piezoelectric Sensor.

Also, the accurate equivalent circuit of the piezoelectric sensor should contain a parallel resistor that creates a leakage path to reduce the charge gradually [16]. Considering this information, the accurate equivalent circuit is shown in Figure 2.4.

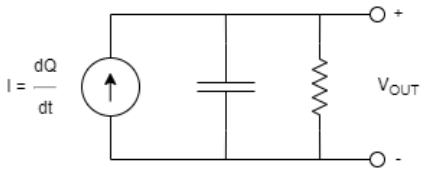

Figure 2.4. The Accurate Model of the Piezoelectric Sensor.

The charge produced by the piezoelectric sensor is in the order of picocoulombs per newton. Therefore, a piezoelectric sensor is generally used with a charge amplifier to convert this charge into a usable voltage level. The charge amplifier which has high input impedance works as an integrator. Thanks to its integration feature, the charge which is generated by the piezoelectric sensor can be converted into usable voltage [17].

In addition to this, high input impedance serves a purpose that charge does not vanish through leakage. The charge amplifier has a capacitance on its feedback path to generate an output voltage that is proportional to the input current which is accumulated over time [17]. The basic configuration of the charge amplifier can be seen in Figure 2.5. The V_{OUT} in Figure 2.5 is expressed as

$$\mathbf{V}_{OUT} = \frac{1}{C_F}\int -I dt = \frac{-1}{C_F}\int \frac{dQ}{dt} dt = \frac{-Q}{C_F}. \tag{2.2}$$

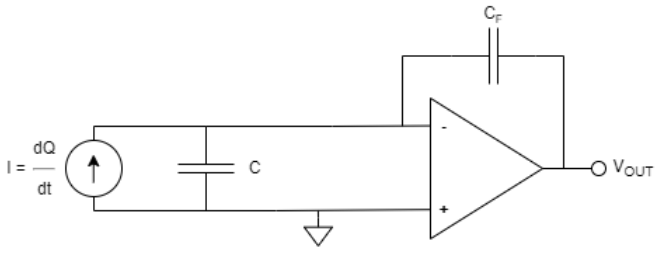

Figure 2.5. The Basic Configuration of the Charge Amplifier.

A more realistic version of the charge amplifier should contain feedback resistor which is connected in parallel with a feedback capacitor to create a discharge path for input bias current to prevent saturation of the amplifier. In addition to this, if the configuration is designed with a single-supply operational amplifier, half of the supply voltage should be applied to the noninverting terminal of the amplifier as an offset voltage [18]. The realistic version of the charge amplifier can be seen in Figure 2.6.

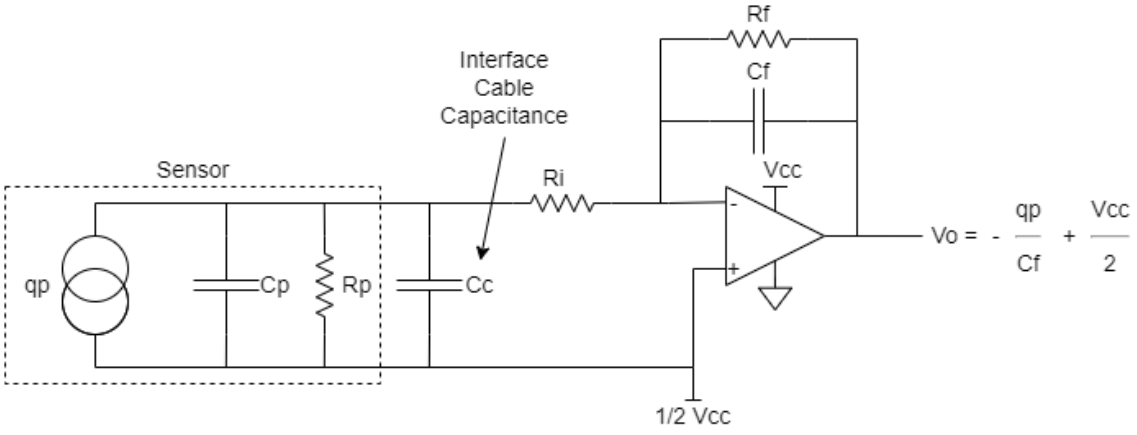

Figure 2.6. The Realistic Model of the Charge Amplifier.

Also, Figure 2.7 shows the frequency response of the charge amplifier. The gain, lower cut-off frequency and higher cut-off frequency, seen in Figure 2.7, can be found as follows:

$$\textbf{Gain} = \frac{1}{C_F}\,, \tag{2.3}$$

$$\mathbf{f}_L = \frac{1}{2\pi C_F R_F}\,, \tag{2.4}$$

$$\mathbf{f}_H = \frac{1}{2\pi R_i (C_p + C_c)}\,. \tag{2.5}$$

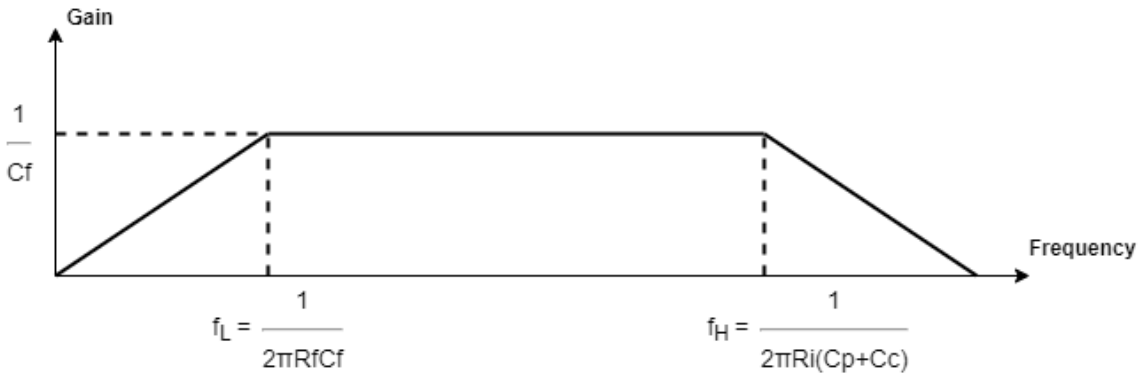

Figure 2.7. Frequency Response of the Charge Amplifier.

In this thesis, LMP7721 IC which has fA level input bias current and very low voltage noise op-amp is used to construct a charge amplifier. The output signal of LDT0-028K and Minisense 100 piezoelectric sensors with high input impedance is amplified using this op-amp [19, 20]. These sensors are shown in Figure 2.8, 2.9, respectively.

Figure 2.8. LDT0-028K Piezoelectric Sensor [19].

Figure 2.9. The Minisense 100 Piezoelectric Sensor [20].

The design started by choosing a feedback capacitance of 8.9 nF. After this selection, the gain was calculated by using (2.3). In order for the low cut-off frequency of 20 Hz, the appropriate feedback resistance was calculated as 1 Mohm by using (2.4). By taking the load capacitance of the used sensor as 480 pF and accepting the cable capacitance as approximately 0.1 nF, the appropriate input resistance was calculated by using (2.5) in order to equate the high cutoff frequency to 600 Hz. The schematic design which can be seen in Figure 2.10 was done by using Altium Designer Tool. Piezoelectric film sensors are used in many studies in order to prevent motion artifacts and get more sensitive results in heart sound analysis systems [21–24]. In all these studies, there is a suitable mechanical structure production to adjust the mechanical stress.

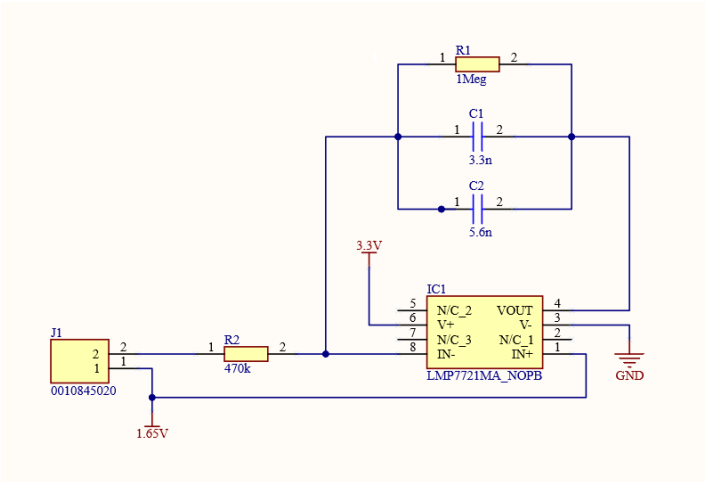

Figure 2.10. The Schematic Design of the Charge Amplifier.

3. HARDWARE DESIGN

The heart sound recording and analysis device, which is the subject of this thesis, consists of subsystems. These subsystems can be seen in Figure 3.1.

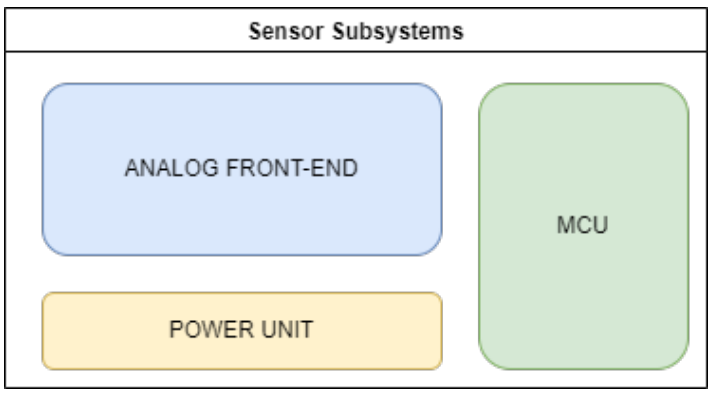

Figure 3.1. Subsystems of the Heart Sound Recording and Analysis System.

3.1. Analog Front-End

First of all, non-stationary phonocardiogram signals with variable frequency and amplitude values, collected by the electret microphone, are amplified in order to analyze them in the analog front-end phase since these signals have very low amplitudes. To process the signal properly, the amplifier and filter are designed at the analog front-end stage.

Figure 3.2 shows the designed analog front-end circuit. In this circuit, the model of the electret microphone, bias stage of the microphone, dc shifter, first order active filter with suitable gain and cascaded 4th order Bessel low pass filter and high pass filter, respectively can be depicted. At the same time, the voltage follower designed to provide the appropriate offset value is also shown in the circuit diagram.

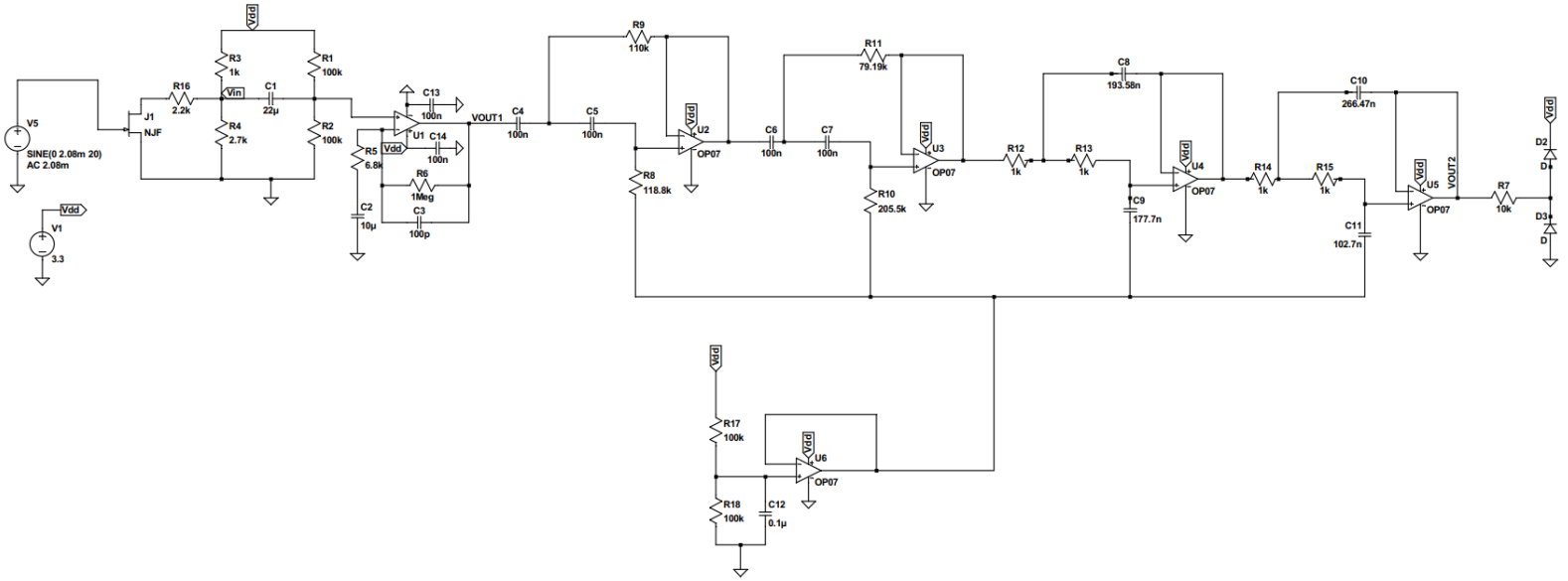

Figure 3.2. The Amplifier and Filter Circuit.

3.1.1. Amplification Stage

In this section, first of all, the POM-5242L-R electret microphone, which has an output impedance of 2.2 kohm and an operating voltage range of 2 V to 10 V, is biased to 2.4 V using a voltage divider [14]. After the microphone is biased, a capacitor is placed in the continuation of the circuit to filter the dc offset and noise below 10 Hz. Rail to rail output MCP6231-E/SN IC, whose gain-bandwidth product is limited to 300 kHz, is used as an opamp in the signal amplification stage [25]. Since this integrated circuit is single-supplied, a DC shifter is placed at the positive terminal of the operational amplifier so that the signal is not distorted. In this way, 1.65 V DC value is applied to the positive input terminal of the opamp through the voltage divider. Therefore, peak to peak voltage of the heart sound signal is prevented from being clipped. The whole system is supplied with a 3.3 V DC supply. In order to boost the heart sound signal with a gain of 146 V/V, the feedback resistors were selected by using gain equation which is expressed as

$$\textbf{Gain} = \frac{R_6}{R_5} + 1\,, \tag{3.1}$$

to provide this gain.

For this part, trimmer potentiometers are used instead of selected resistors in order to change the gain according to the application. Furthermore, for the purpose of ensuring the system can act as unity gain in DC, a capacitance of C_2 has been added to the circuit in series with the R_5 resistor. If this capacitor is not connected to the circuit, the DC offset is amplified, and the signal is clipped due to the supply voltage limitation. With this added capacitance, the cutoff frequency of the high-pass filter is determined. For this reason, the value of this capacitance has been chosen to have an approximately 2 Hz cutoff frequency at the high pass filter stage. On the other hand, the capacitance C_3 determines the cutoff frequency of the low-pass filter. At this stage, it is sufficient to set the cutoff frequency to 1.5 kHz because the signal will then

be filtered again with a sharper filter to capture the 20-600 Hz heart sound frequency range. For this reason, C_3 was set according to this cutoff frequency. Cutoff frequencies are found as follows:

$$\mathbf{f_c} = \frac{1}{2 * \pi * R * C}\,. \tag{3.2}$$

C_{13} and C_{14} capacitors were placed on the Vdd and Gnd lines for decoupling. Lastly, protection diodes were placed at the end of the amplification stage [26].

3.1.2. Filtering Stage

As explained in Chapter 1, normal and abnormal heart sounds have a minimum frequency range of 20 Hz and a maximum of 600 Hz. For this reason, signals lower than about 20 Hz and higher than 600 Hz are eliminated from the signal by cascading the fourth-order unity gain high-pass Bessel filter and the fourth-order unity gain low-pass Bessel filter to use the signal correctly in the next stages. The phonocardiogram signal contains S1, S2, S3 and S4 sounds which have different frequency components [27].Non-linearly changing phase components undergo different delays while passing through the filter, which can cause phase distortions of the signal. This may cause misinterpretations later when the features of the signal are extracted. For this reason, the Bessel filter is preferred as the filter in order to ensure that the phase shift of the signal is linear for all frequency components [28].

While cascaded fourth order Bessel filter is designed, MCP604 quad opamp was used to provide minimum area usage. This opamp has low input bias current, single supply, high speed working and rail-to-rail output swing specifications [29]. In order to prevent distortion of the input signal due to the filter's single supply specification, the output signal has an offset value of 1.65 V DC thanks to the designed voltage follower circuit which is connected to the filter. The unity-gain second order Sallen-Key topology which is illustrated in Figure 3.3 and Figure 3.4 was used in the filter design. The values of the components utilized in the filter were found using the table

in Figure 3.5 and equations given below, respectively. Firstly, by using Figure 3.5, f_{01}, Q_1 , f_{02} and Q_2 were found 1.419, 0.522, 1.591 and 0.806 for n which is equal to 4, respectively.

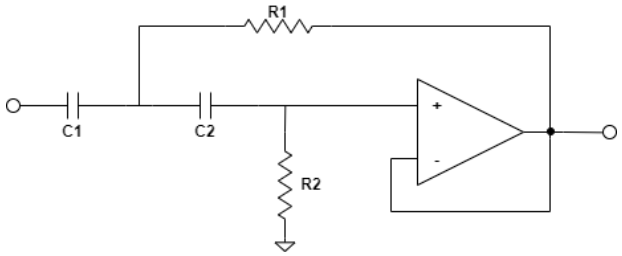

Figure 3.3. Sallen Key High Pass Filter Topology.

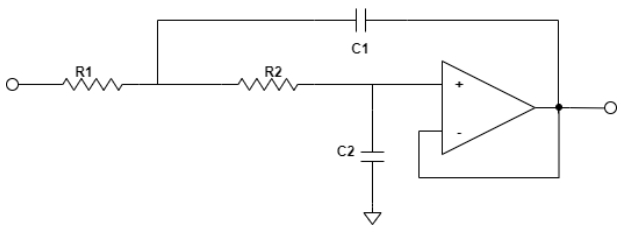

Figure 3.4. Sallen Key Low Pass Filter Topology.

n	f_{01}	Q_1	f_{02}	Q_2	f_{03}	Q_3	f_{04}	Q_4	f_{05}	Q_5
2	1.274	0.577								
3	1.453	0.691	1.327							
4	1.419	0.522	1.591	0.806						
5	1.561	0.564	1.760	0.917	1.507					
6	1.606	0.510	1.691	0.611	1.907	1.023				
7	1.719	0.533	1.824	0.661	2.051	1.127	1.685			
8	1.784	0.506	1.838	0.560	1.958	0.711	2.196	1.226		
9	1.880	0.520	1.949	0.589	2.081	0.760	2.324	1.322	1.858	
10	1.949	0.504	1.987	0.538	2.068	0.620	2.211	0.810	2.485	1.415

Figure 3.5. The Tabulated Data for Normalized Bessel Filter [30].

Then, two second order active high pass filters with the unity gain and two second order active low pass filters with the unity gain were designed as cascaded, where

$$\mathbf{H_{OHP}} = 1\,V/V, \tag{3.3}$$

$$\mathbf{f_{0HP}} = \frac{f_c}{f_{0(Figure\,3.5)}}, \tag{3.4}$$

$$\mathbf{n} \geq 4Q^2, \tag{3.5}$$

$$\mathbf{k} = \frac{n}{2Q^2} - 1, \tag{3.6}$$

$$\mathbf{m} = k + \sqrt{k^2 - 1}, \tag{3.7}$$

$$\mathbf{Q_{HP}} = \frac{\sqrt{\frac{n}{m}}}{n+1}, \tag{3.8}$$

$$\omega_\mathbf{0} = \frac{1}{\sqrt{mn}RC}, \tag{3.9}$$

$$\mathbf{R} = \frac{1}{\sqrt{mn}2\pi f_0 C}, \tag{3.10}$$

$$\mathbf{H_{OLP}} = 1\,V/V, \tag{3.11}$$

$$\mathbf{f_{0LP}} = f_{0(Figure\,3.5)} * f_c, \tag{3.12}$$

$$\mathbf{Q_{LP}} = \frac{\sqrt{nm}}{m+1}. \tag{3.13}$$

For simplicity, the components were accepted as $C_1 = nC_2$, $R_1 = mR_2$, $C_2 = C$ and $R_2 = R$. Finally, 4th order Bessel bandpass filter has been constructed after calculating capacitor and resistor values. These values can be seen in Table 3.1 and 3.2.

Table 3.1. Fourth Order High Pass Bessel Filter Component Values.

	R_1	R_2	C_1	C_2
First Stage	110 kΩ	118.8 kΩ	100 nF	100 nF
Second Stage	79.2 kΩ	205.5 kΩ	100 nF	100 nF

Table 3.2. Fourth Order Low Pass Bessel Filter Component Values.

	R_1	R_2	C_1	C_2
First Stage	1 kΩ	1 kΩ	193.6 nF	177.7 nF
Second Stage	1 kΩ	1 kΩ	266.5 nF	102.7 nF

Since the quad opamp used is a single supply opamp, a fixed offset is provided with the voltage follower designed for the system. This offset value of 1.65 V is provided by a voltage divider using R_{17} and R_{18} resistors. In this way, clipping of the maximum and minimum voltage values of the signal is prevented. AC analysis of the amplifier and filter was done by using LTSpice. The simulation results are shown in Figure 3.6. In this figure, the green plot represents first stage response, the red plot represents the second stage response and the blue plot represents the overall transfer function of the filtering part. The PCB design of this circuit was done by using Altium Designer. Besides, constructed schematic design by using this software can be seen in Figure 3.7.

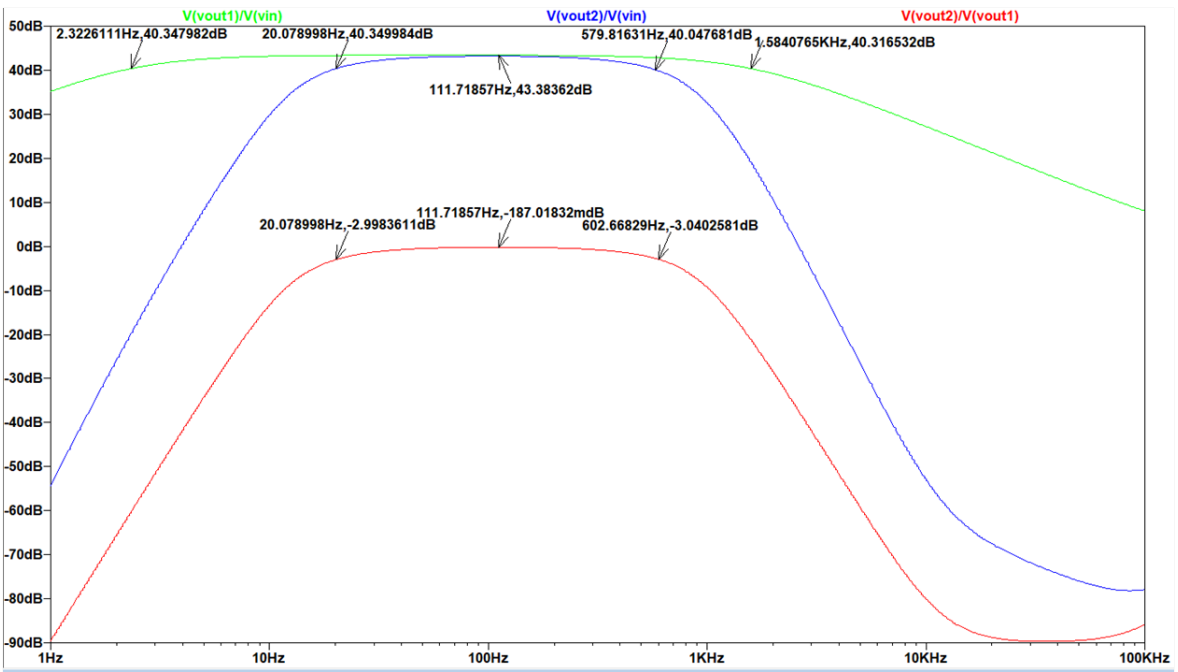

Figure 3.6. AC Analysis of the Amplifier and Filter Circuit.

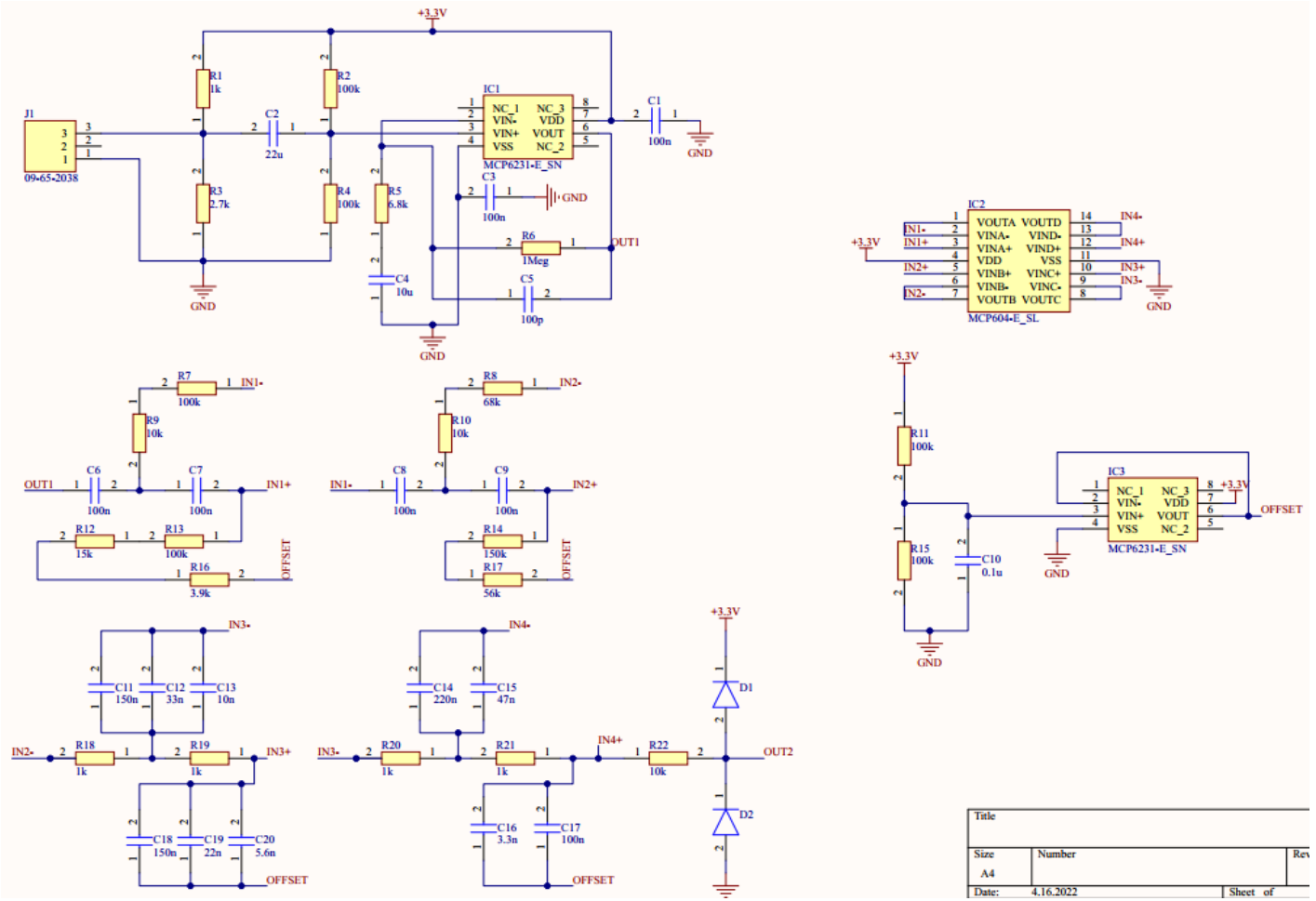

Figure 3.7. The Schematic of the Amplifier and Filter Circuit.

After these stages were designed, the system's constant supply voltage is provided by using linear voltage regulator that is produced by Texas Instruments. For this purpose, TPS73633 IC was used to fix the supply voltage at 3.3 V DC. For the input voltage range of 1.7 V to 5.5 V, TPS73633 produces a fixed voltage of 3.3 volt which is required for supplying the whole system. This integrated circuit is used to ensure that the system is supplied with a constant voltage instead of supplying directly with a Lithium-ion battery which has an unstable voltage value. It has 75 mV low voltage drop and uses a configuration has a voltage follower with NMOS pass transistor in it [31]. Figure 3.8 demonstrates the schematic of the voltage regulator which is used in the design.

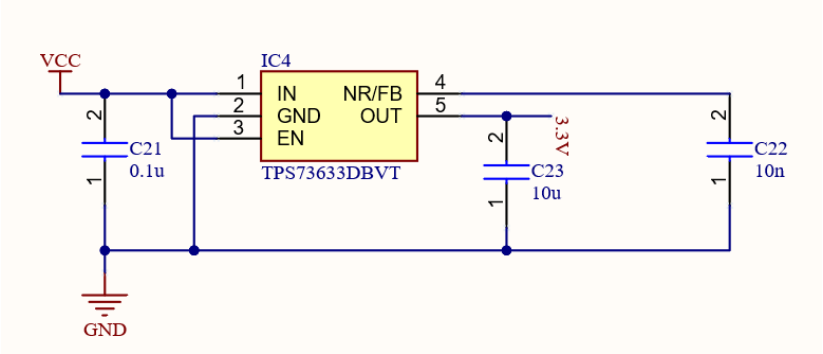

Figure 3.8. The Schematic of the Voltage Regulator.

3.1.3. Audio Power Amplification Stage

An audio power amplifier has been used to allow the people who will use the sensor to listen to the heart sound with a headphone output while recording the heart sound. For this reason, the LM4875 integrated circuit is used to amplify the low-power heart sound signal from the filter output to high levels so that headphones or loudspeakers can be driven [32]. Thanks to this integrated circuit, people can listen to heart sounds at desired levels, adjust the volume and identify the points where they get the best sound by using the volume control feature with a mono headphone. After this control, they can start recording their heart sounds in the most accurate way. Figure 3.9 demonstrates the schematic of the voltage regulator which is used in design.

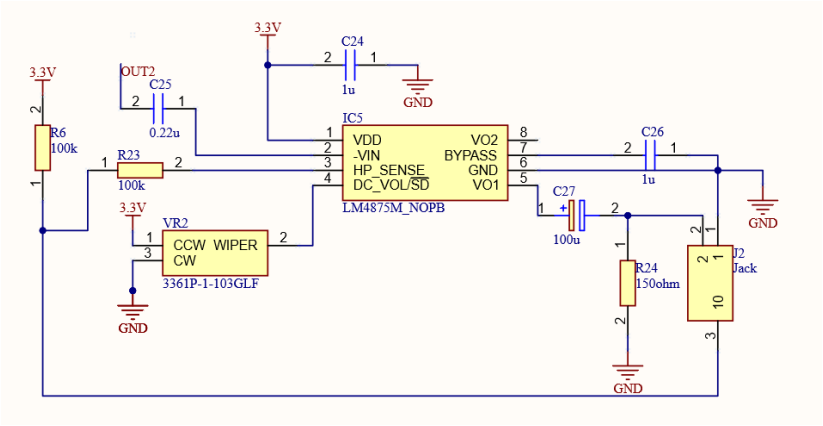

Figure 3.9. The Schematic of the Audio Power Amplifier.

3.1.4. Overall PCB Design

The circuit which has been designed in two layers is printed on Rodgers material. The dimensions of the circuit are measured as 87 mm x 65 mm. The designed PCB includes a microphone bias circuit, an amplification circuit, filtering circuit, voltage follower, voltage regulator, a power amplification circuit, and headers. Overall circuit design schematic and its 3D model which are created by using the Altium Designer tool are shown in Figure 3.10 and Figure 3.11, respectively. The final printed circuit board is shown in Figure 3.12.

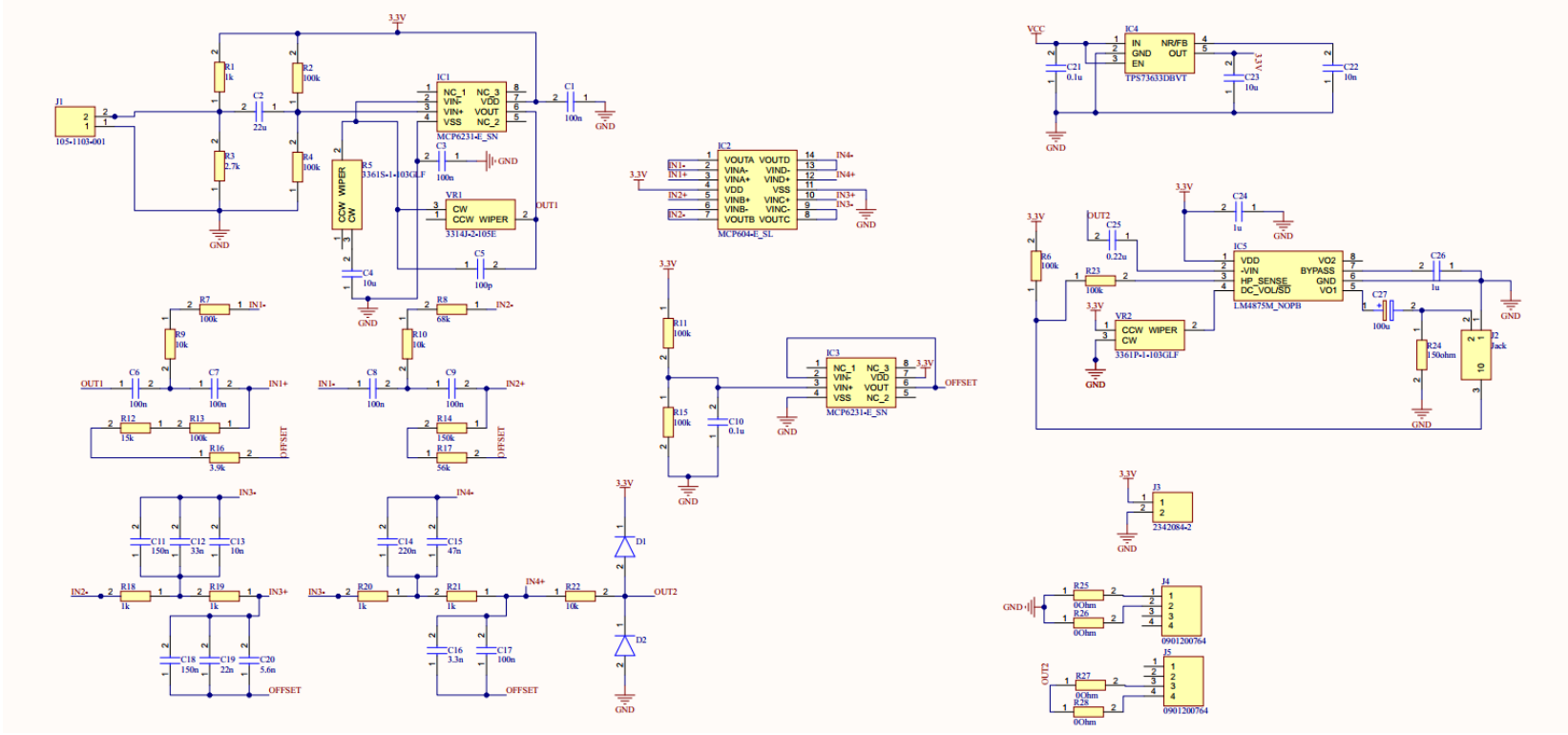

Figure 3.10. The Schematic of the Overall Circuit Design for Heart Sound Acquisition and Analysis System.

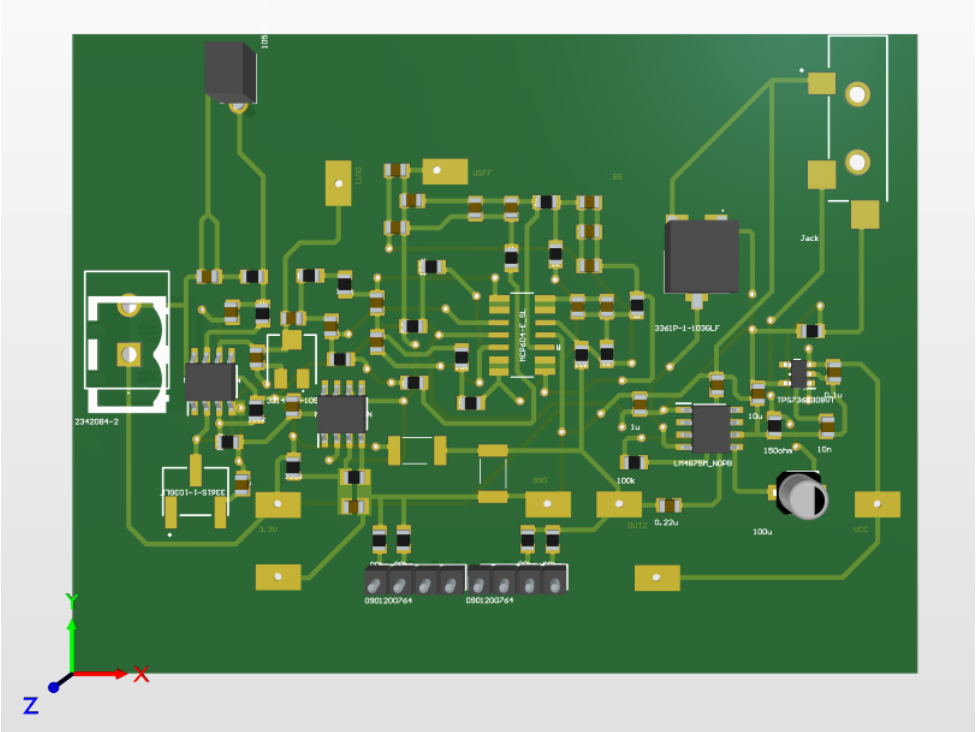

Figure 3.11. The 3-Dimensional Model of the Designed Circuit.

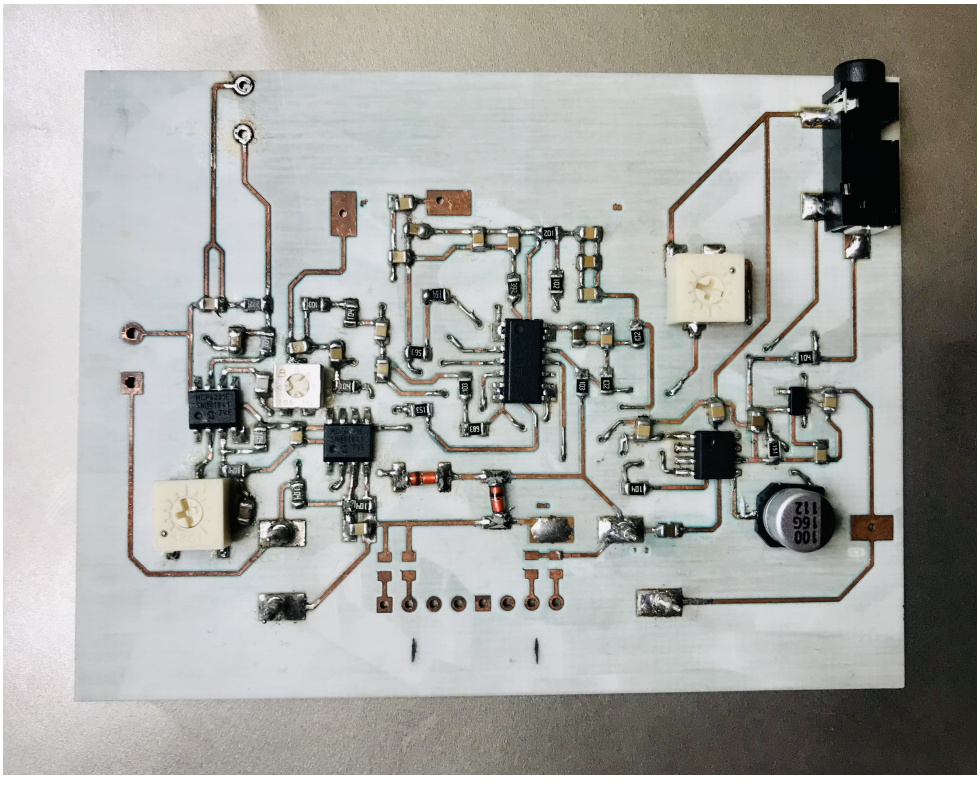

Figure 3.12. The Final PCB Design.

3.2. The Results of Different Data Acquisition Methods

In this thesis, heart sounds are acquired using four different experimental setups which can be seen in Figure 3.13. In order to adjust the appropriate gain values for each application the feedback resistors are changed by using the trimmer potentiometers in the amplification section and the results are observed.

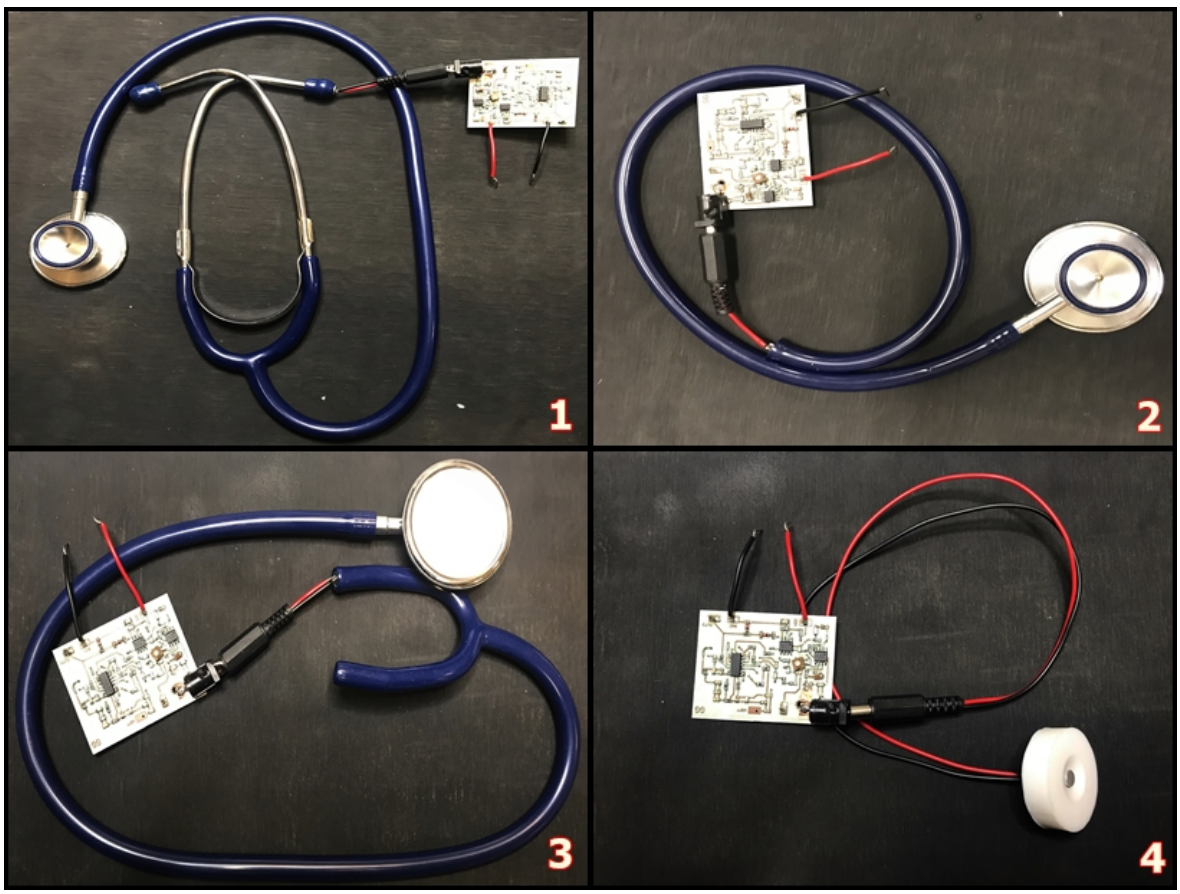

Figure 3.13. The Setups of the Heart Sound Acquisition System (1: Whole Acoustic Stethoscope, 2: Single Channel Flexible Tube, 3: Double Channel Flexible Tube, 4: Microphone Capsule).

First of all, in setup 1, the system is established by placing an electret microphone on one of the earpieces of the stethoscope without deforming the structure of the acoustic stethoscope. The phonocardiogram signal which is obtained with this data collection mechanism is shown in Figure 3.14.

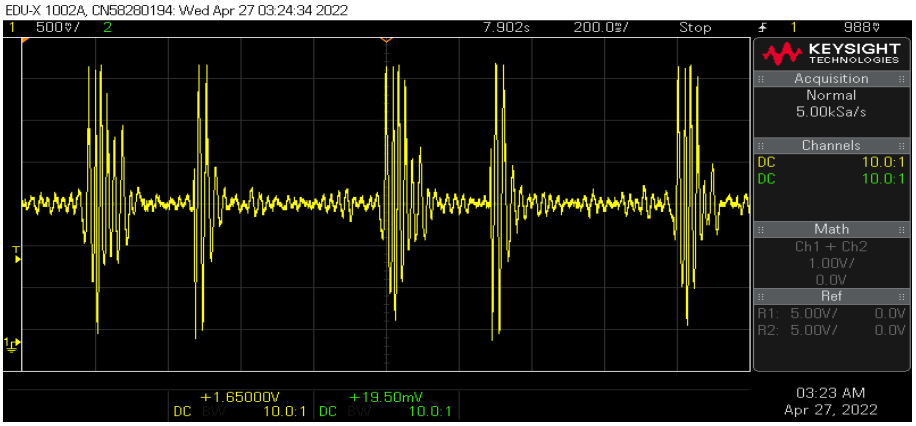

Figure 3.14. The Acquired Heart Sound Signal with First Established Setup (200 ms Time Division, 500 mV Voltage Division).

In the second data collection setup, an electret microphone is placed at the end of the stethoscope single tube and a heart sound signal is obtained by using the acoustic stethoscope diaphragm. The acquired signal is shown in Figure 3.15.

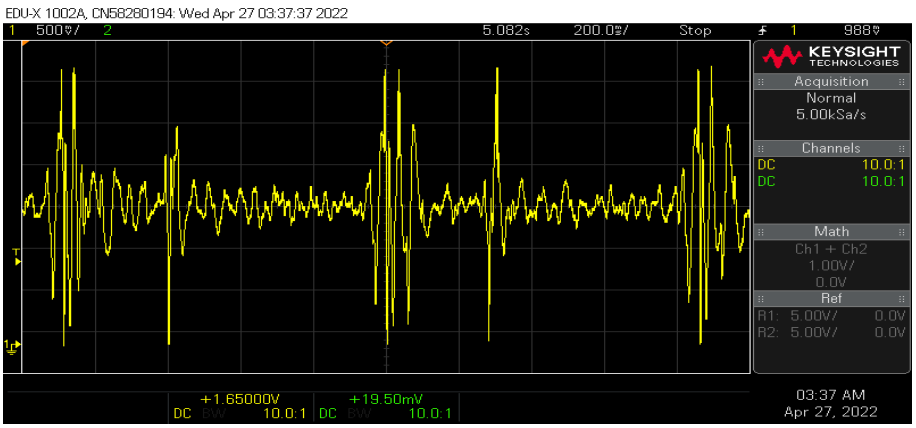

Figure 3.15. The Acquired Heart Sound Signal with the Second Established Setup (200 ms Time Division, 500 mV Voltage Division).

In the third data collection setup, the stethoscope tube is used as a double channel. An electret microphone is placed in only one of the channels and the heart sound signal at the filter output is obtained. The results can be seen in Figure 3.16.

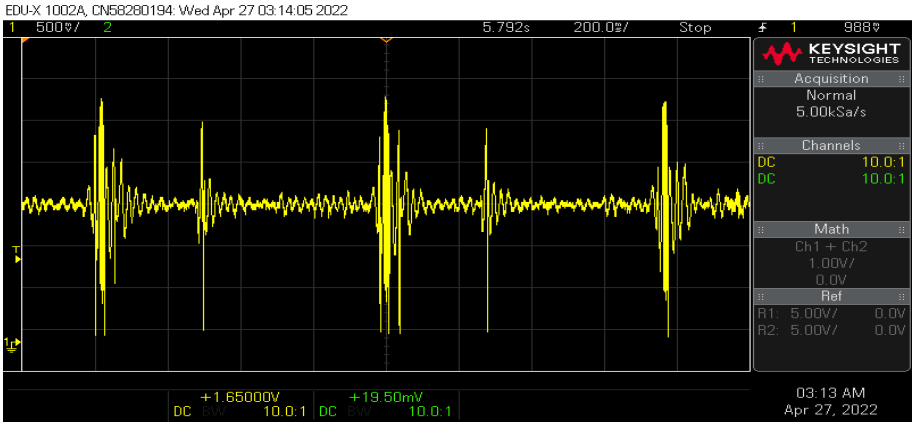

Figure 3.16. The Acquired Heart Sound Signal with the Third Established Setup (200 ms Time Division, 500 mV Voltage Division).

Finally, the heart sound signal is procured by placing an electret microphone inside the microphone capsule produced in Boğaziçi University Lung Acoustic Laboratory (LAL). Results are obtained by using the fourth data acquisition setup shown in Figure 3.17.

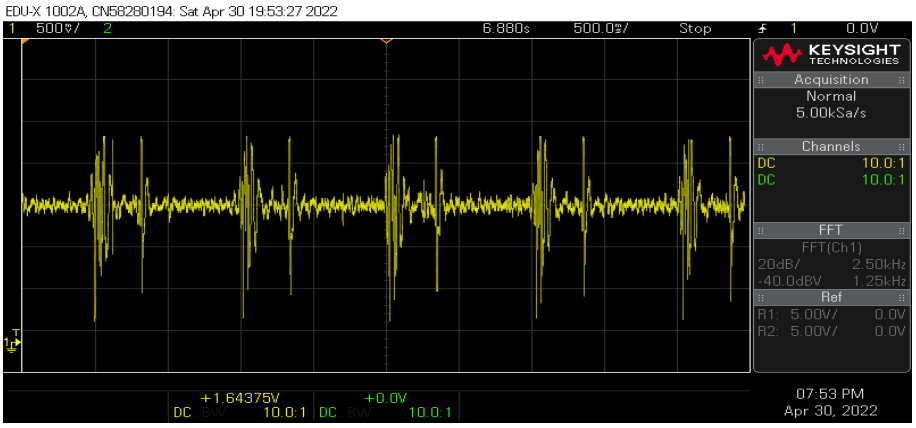

Figure 3.17. The Acquired Heart Sound Signal with the Fourth Established Setup (500 ms Time Division, 500 mV Voltage Division).

In addition to these, the systole and diastole times in one cardiac cycle are examined. The heart sound signal obtained by averaging about 8 recorded cardiac cycles can be seen in Figure 3.18. The obtained one cardiac cycle lasts approximately 800 ms. This time is divided into the systole time which is found as 330 ms and the dias-

tole time which lasts 470 ms. These times were found to be consistent with the times specified in the literature for an average heart rate.

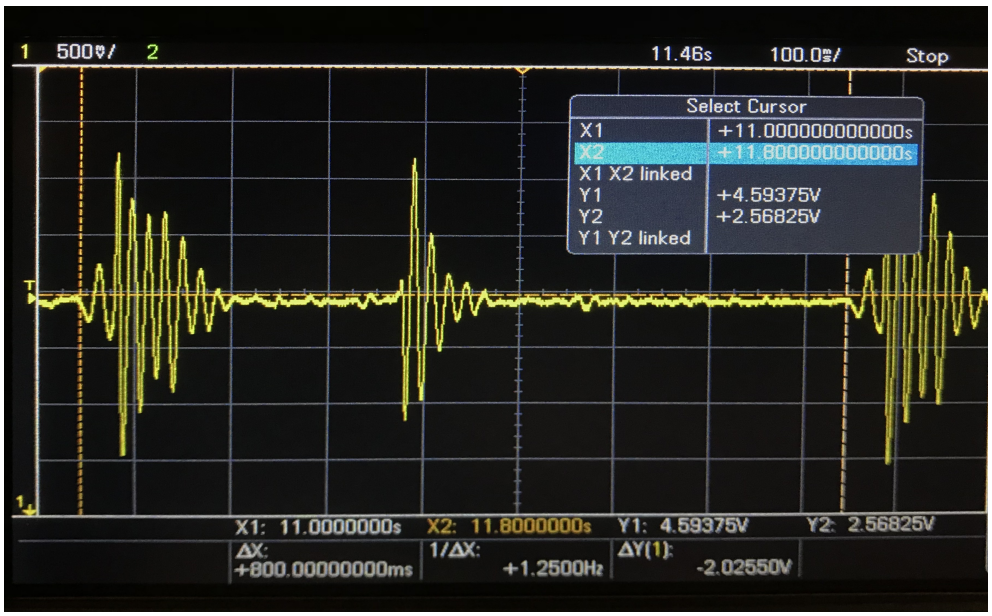

Figure 3.18. The Average of the Cardiac Cycle of the Taken Heart Sound.

As seen in the figures, the S1 and S2 peaks of the heart sound signal received by all data acquisition setups can be detected in a distinctive way. The signal received with any of these methods can be easily used in the subsequent signal processing processes for segmenting the signal and extracting the time domain components.

4. EMBEDDED SYSTEM ARCHITECTURE

In this thesis, the nRF52832 development kit is used to convert analog heart sound signals to digital and to send the data to computer and phone over Bluetooth Low Energy. SEGGER's Embedded Studio is used to program this development kit. Thanks to the ADC in the microprocessor, the phonocardiogram signal is sampled with 12-bit resolution and 1.25 kHz sampling frequency. In this way, an external high-speed ADC is not required in this system, and the level of cost and complexity is reduced. The power consumption can be kept at a lower level and sample losses that may occur in cases where the ADC speed and the data transfer rate do not match are prevented. In this way, the length of data recording is not limited and the heart sound signal is transferred to the computer and phone in real-time with one of the wireless technologies, BLE. The nRF52832 microprocessor, which is frequently used in wearable sensor technologies, low-energy audio signals transmission, medical sensor technologies and various IoT systems, has a large memory feature. In addition to containing many protocols, it is especially preferred in BLE applications [33, 34] . The aforementioned development kit and its block diagram are shown in Figure 4.1 and Figure 4.2, respectively.

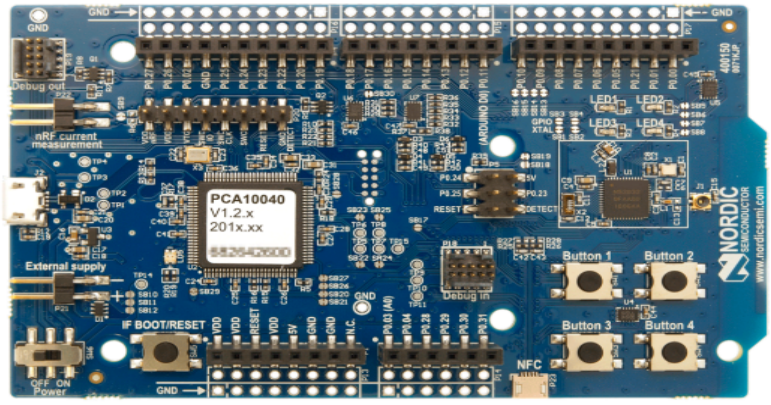

Figure 4.1. nRF52832 Development Kit [34].

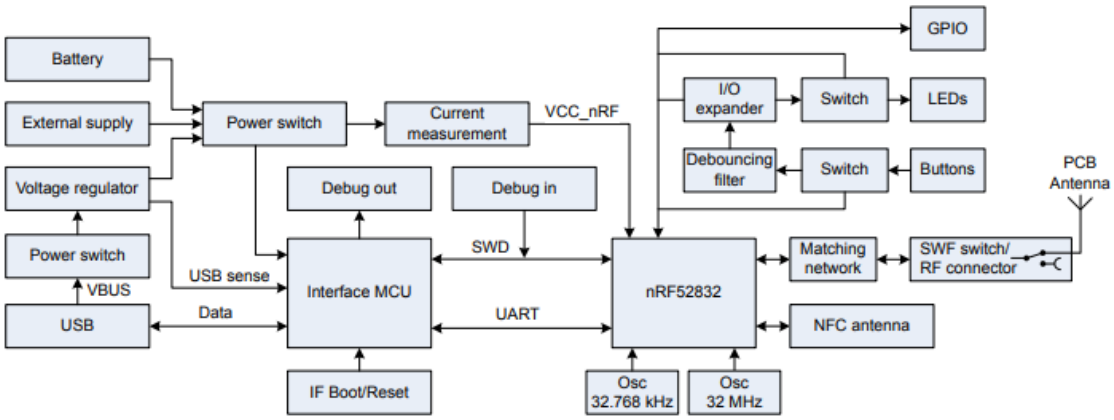

Figure 4.2. The Block Daigram of the Nrf52832 DK [34].

4.1. SAADC

First of all, the filtered analog signal is converted into a digital signal by using SAADC block in nRF52 DK in this section. Differential SAR ADC is used for this part. The signal is sampled with 12-bit resolution and 1250 Hz sampling rate. Samples which are taken can be transferred to the 32 kB RAM or directly [35]. SAADC block contains sample and hold circuit, digital to analog converter, comparator and successive approximation register circuits in it. One of the types of ADCs used to convert a continuous analog signal to digital is SAR ADCs. First, a sample-and-hold circuit is used to sample the input voltage. After this process, the successive approximation register is initialized with the most significant bit being 1. This digital code is converted to analog by the DAC. This value and the input voltage are compared by the comparator and its output is sent to the SAR. If this value is greater than the input voltage, that bit is reset by the SAR, otherwise, it is not changed and this comparison process is repeated for all bits until the end of the conversion [36, 37]. The analog-to-digital converter has a timer that can provide a continuous sampling. Thus, there is no need for the external timer. In this way, the signal coming from the analog input pin is continuously sampled and kept in a buffer. When the buffer is full, the digital data is sent to the computer via BLE thanks to an incoming interrupt.

To find the resultant voltage, some parameters are set first. These parameters are gain, reference voltage, resolution and mode of operation. In this part, the gain value is set to 1/4, the reference voltage is set to Vdd/4, bit resolution is chosen as 12 bit and mode of operation is preferred as single-ended [35]. By using these parameters, binary voltage values (V_b) which means the obtained digital sample equivalent of the analog voltage value of the signal and input range are found as follows:

$$\textbf{Input Range} = \frac{Reference\,Voltage}{Gain} = Vdd, \tag{4.1}$$

$$\mathbf{V_b} = V_{input} * \frac{Gain}{Reference\,Voltage} * 2^{Resolution-m}. \tag{4.2}$$

In (4.1) and (4.2), m is equal to 0 for a single-ended operation. After the known values are replaced, the binary voltage value can be determined as

$$\mathbf{V_b} = \frac{V_{input}}{Vdd} * 2^{12}. \tag{4.3}$$

4.2. Bluetooth Low Energy

Bluetooth Low Energy technology, which is one of the types of wireless communication, has been preferred as a communication method especially due to its high data transfer rate which is 1 Mbps or 2 Mbps and low power consumption which is equal to maximum of +4 dBm during transmission. Data transmission is provided as notifications from server to client. Thus, there is no need to acknowledgment data from the client. The operation frequency band of the BLE is equal to 2.4 GHz. In addition to these features, the power consumed by this development kit for data transmission ranges from -20 dBm to +4 dBm, depending on the size of the data packet and the sending distance. [33]. In this thesis, the analog heart sound signal, which is converted to digital, is transmitted to the computer and the smartphone via Bluetooth Low Energy with the interrupt that comes after the buffer which is set to hold 3 samples is filled. Connection parameters are set as 8 ms as minimum connection interval, 100 ms

as maximum connection interval and 4 seconds as supervision timeout, respectively. Communicating with the low-cost nRF52840 USB Dongle, the nRF52832 DK sends digital data which holds in a hexadecimal format directly to the Nordic Semiconductor's software tool which is called nRF Connect via this dongle which can be seen in Figure 4.3 [38].

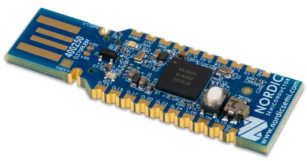

Figure 4.3. The nRF52840 Dongle [38].

On this interface, the transmitted samples can be observed in real-time and are also stored in txt format. This interface and connection structure can be perceived in Figure 4.4. The nRF52 is supplied by using a 3.3 V voltage regulator as in the hardware design. During the measurements, the current drawn by the system is measured as 5 mA while data transmission is provided. The maximum power consumption calculated for the digital part is found to be 16.5 mW during the data transmission via BLE.

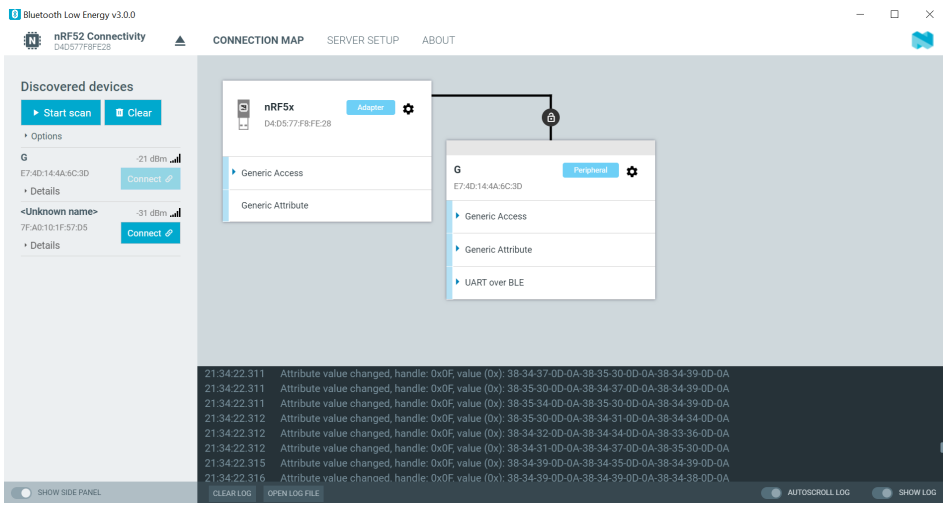

Figure 4.4. The nRF Connect Tool Interface.

5. SOFTWARE DESIGN

5.1. Data Acquisition

Firstly, the heart sound signal is collected from volunteers to use in the signal processing stages. In this part, participants are requested to place the stethoscope diaphragm on the mitral region of the chest to record the amplified and filtered heart sound signal during the preprocessing in a quiet environment. At the same time, while the heart sound signal is recorded, participants listen to this sound with headphones. Participants whose heart sound recordings are used in this study are asked to fill out an ethics committee form which was approved by decision No. 2022/12. The signal is transferred afterward to MATLAB in hexadecimal format from the nRF connect software. This signal is then passed through a series of signal processing processes by using MATLAB.

5.2. Signal Processing

Phonocardiogram, being a non-invasive method, has an important place in heart sound signal analysis. The heart sound signal, which is passed through signal processing processes, can be analyzed much more accurately than the classical auscultation method. The heart sound signal collected by the sensor produced in this thesis can be listened to on the created interface, examined visually, and analyzed by passing through certain signal processing stages. As a result, the person's heart rate, heart rate variability and abnormal characteristics of the heart sound are checked. In this section, heart sound normalization, feature extraction, segmentation, HR and HRV calculation and N/ABN decision mechanism are examined respectively.

In order to extract meaningful information from the heart sound signal, the sound signal must first be segmented regardless of whether it is received from a healthy or unhealthy person. This segmentation process is performed by using features in the time domain, frequency domain, or both, extracted from the heart sound [39]. The

aim of this section is to find the S1-S2 peaks of the signal and to separate the times between these peaks as systole and diastole [40]. In the analysis part of the system, the segmentation is done by extracting the Shannon energy envelope, which is the time domain feature attributed in the literature [41]. Then, the Fast Fourier Transform and Hilbert Huang Transform of the signal are examined to create a decision mechanism. In Figure 5.1, these processes can be seen, respectively.

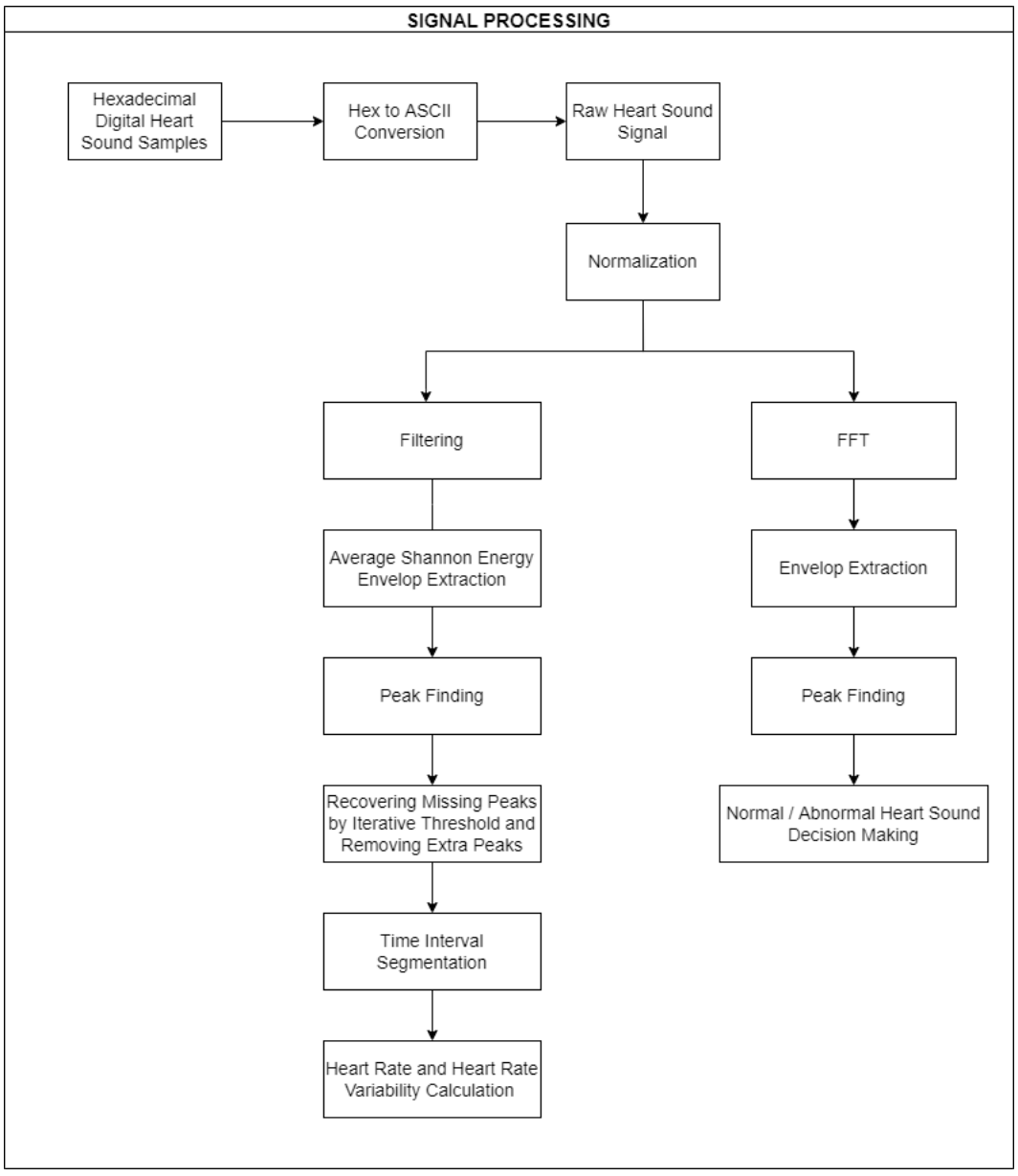

Figure 5.1. The Signal Processing Stages of the Heart Sound Analysis System.

5.2.1. The Shannon Energy Envelope

First of all, in order to convert the signal sent to the computer in hexadecimal format into meaningful digital samples, it first takes the digital number values thanks to the automatic hexadecimal to ASCII conversion function created in this study. Thanks to this function constituted, firstly the lines containing the relevant digital sample values are extracted from the file saved in text format via the nRF Connect software. Then, each value is converted to its numerical equivalent with the help of the created hexadecimal to the ASCII table, with values from 0 to 4096 for 12 bits. The digital values obtained in this section are converted to voltage equivalents and the raw data is plotted during the recording period. After the raw data is obtained, the signal normalization is first done according to its maximum amplitude so that the segmentation can be done correctly. For this purpose, normalized signal is written as

$$\mathbf{x(k)_{Normalized}} = \frac{x(k)}{max(|x(i)|)}, \tag{5.1}$$

where x, k and i represent the raw heart sound signal, number of sample and sample number where the maximum peak location, respectively was used. After normalization, Chebyshev type 1 bandpass filter with 20 Hz to 300 Hz cutoff frequency is applied to remove the noise remaining. This filter is preferred in order to provide steep filter response.

Then, the average Shannon energy of the signal is calculated so that the obtained signal can be segmented into the basic components of the first HS, second HS, systole and diastole time intervals. On this energy envelope, the positions of the first heart sound and the second heart sound on the signal and their amplitudes at those positions are extracted. In the next step, the systole and diastole time intervals between consecutive peaks are determined by the created algorithm. The Shannon energy feature is preferred for this phase because it accentuates medium-intensity peaks more. In this way, the effect of low amplitude noise can be avoided [41].

Firstly, the Shannon energy of the normalized signal is found as follows:

$$\mathbf{E} = -x^2 * log\, x^2. \tag{5.2}$$

This signal is then divided into windows of 20 ms length to capture peaks properly and its average Shannon energy is calculated as

$$\mathbf{E_{Average}} = \frac{-1}{N} * \sum_{i=1}^{N} (x(i))^2 * log\, (x(i))^2. \tag{5.3}$$

Finally, the result is normalized with respect to its mean and standard deviation values [41]. The normalization of the energy is calculated as follows:

$$\mathbf{E_{Normalized}} = \frac{E_{Average}(t) - M(E_{Average}(t))}{S(E_{Average}(t))}, \tag{5.4}$$

where E, N, M, and S represent the Shannon energy, number of sample per window, mean and standard deviation, respectively.

After the normalized Shannon energy is calculated, the first peak (S1) and the second peak (S2) locations and amplitudes at this location are found above the threshold value which is set by using the peak finder function in MATLAB. Raw data which is taken from the volunteer and its Shannon energy envelop are illustrated in Figure 5.2. S1 and S2 peaks which are found with respect to this graph can be seen in Figure 5.3.

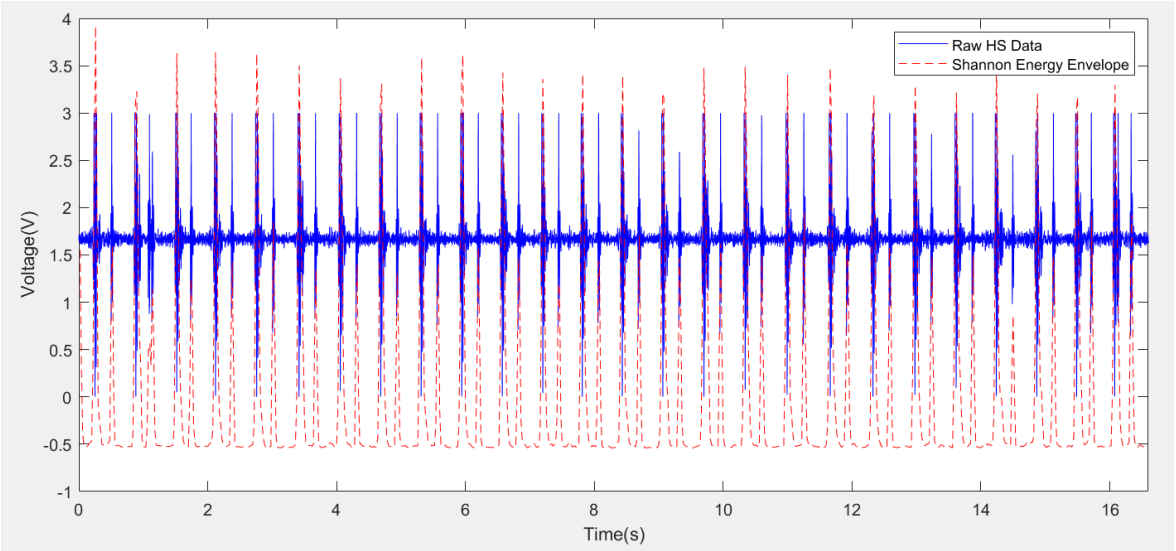

Figure 5.2. The Raw Heart Sound Signal and Averaged Shannon Energy.

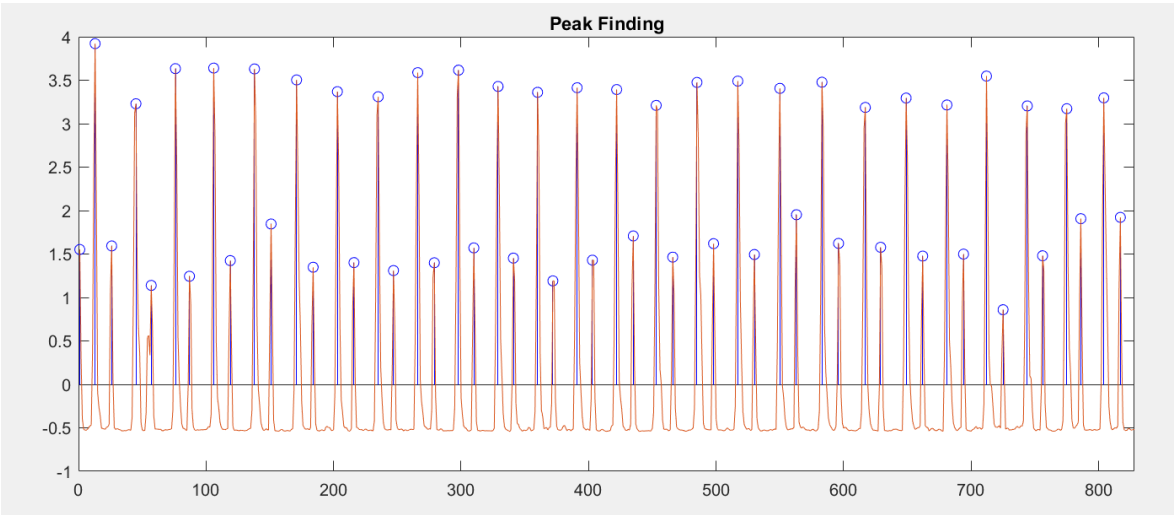

Figure 5.3. Detection of the S1 and S2 Peak Locations and Amplitudes.

5.2.2. The Peak Recovering and The Peak Removing

During the peak finding process, peaks above the specified threshold value are found by using the peak finder function. For this process, the threshold value is changed iteratively to prevent the analysis system from missing the peaks. First, the peak at the maximum amplitude is found from the average Shannon energy graph and the iteration is started with 10 percent of this peak amplitude value. Then, during each

peak detection process, the specified threshold value is reduced by 200 mV and peak detection is performed again. This process is continued until there is no change in the number of newly found peaks. Thus, the possibility of the system to miss peaks is reduced to a minimum. The intervals between the peaks whose positions are determined are found by subtracting the positions of the consecutive peaks. And this process is applied throughout the entire signal. Then, the average of the obtained time interval values is calculated. Consequently, intervals below this average are defined as systole, and intervals above this average are defined as diastole [41].

Afterward, the distributions based on their standard deviations are determined for the systole and diastole. The intervals that do not fall within this distribution indicate a false peak found. For this reason, the systole and diastole times that are outside the upper and lower ranges of the mean by the standard deviation are determined. The intervals between successive peaks are then compared with the this determined interval lengths. If these interval times are equal, it means that one of the peaks determined here is an extra peak. Therefore, the smaller peak between consecutive peaks is labeled as the extra peak and deleted [41]. Thus, false peaks are removed from the peak sequence. The results of the algorithm developed to prevent peak missing and also to remove incorrectly found extra peaks from the sequence are shown in Figure 5.4.

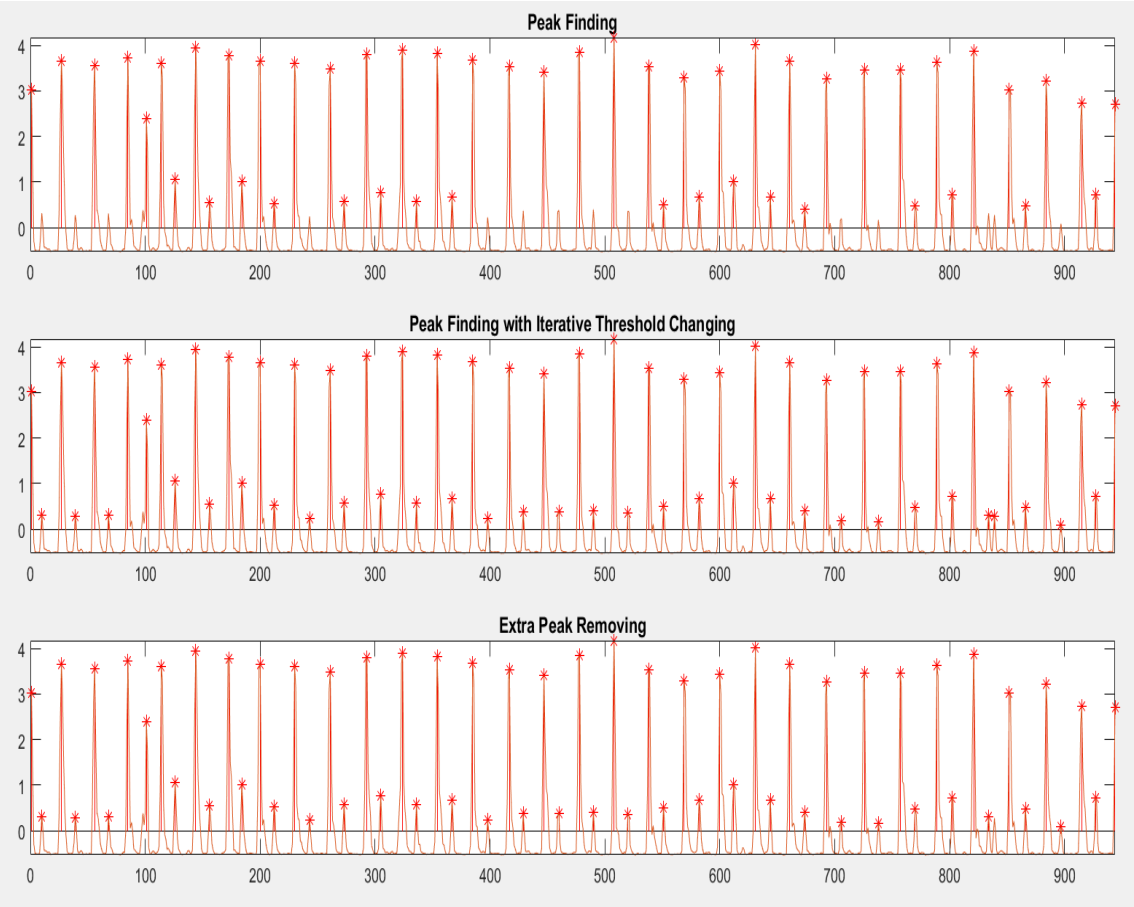

Figure 5.4. The Peak Recovering and Elimination of the Extra Peaks.

5.2.3. The Heart Rate and The Heart Rate Variability Calculations

Heart rate data, which is the first measured value during the control of people's heart health conditions, provides a quick opportunity for healthcare professionals to see if there is a condition that may threaten the individual's heart health. In addition, by examining the variability of the heartbeat time intervals of people, it is possible to make comments about their autonomic nervous systems. People can make these measurements at their homes easily with the technological health devices developed. Heart rate (HR), which is very simple to measure, is the expression of the person's average heartbeat in 1 minute. It usually reaches high values during brisk activities and is around 60-100 beats per minute at rest. On the other hand, heart rate variability (HRV) is related to the time variability of the heart beats in each cycle. Heart rate variability data allow assessment of individuals' stress tolerance [42].

In this thesis, while the heart sounds are recorded and analyzed with the designed instrument, it is also possible for people to easily access and record heart rate and heart rate variability data in the system. First of all, the average heartbeat duration is calculated over the whole heart sound signal, and later the data on how many heartbeats will be taken in 60 seconds with obtained average duration is determined. This data shows the heart rate value in beats per minute. On the other hand, the average difference between consecutive heartbeat temporal locations gives a heart rate variability value. HRV is divided into 3 sub-classes depending on the recording periods taken. The first of these is ultra short term HRV, this is the value extracted from the heart sound recordings of 30 seconds or less. The other is the short-term HRV (STV) which refers to the value calculated from the records taken during 5 minutes. There is also long-term HRV (LTV) calculated from recordings of 24 hours or more taken to more accurately diagnose cardiac disorders. It is aimed to shorten the heart sound or ECG recording and HRV calculation duration in order to facilitate integration with medical devices that can be used at home or wearable medical sensors. For this reason, HRV values that can be calculated with high accuracy in less than 5 minutes are being integrated and tested in medical systems today [43, 44]. This variability value can be measured in 4 different ways. The first of these is the measurement based on the standard deviation. The second calculation method is to calculate the RMS value of consecutive interval differences.

While calculating STV, the method applied in this thesis is to calculate the average value of the absolute differences of consecutive cardiac cycles' time intervals. Finally, the method used when calculating LTV is to take the mean of the variation between the longest and shortest cardiac cycle intervals of the 1-minute segmented data. HRV data can warn that a person may have some disorders, such as pulmonary diseases, hypertension, asthma, inflammation, and arrhythmia. It may also contain information about the person's psychological state, such as stress disorder, anxiety, and depression. For this reason, it is of great importance that it can be measured with health devices that are easy to use and access [43].

5.2.4. The Detection of the Normal and Abnormal Heart Sounds

In the previous section, Shannon energy, which is the time domain feature of the signal, was examined to separate the PCG signal into time intervals. In addition to this method, which is widely used in normal heart sound segmentation, it is possible to detect whether there is an abnormality in the signal by examining the frequency and time-frequency domains of the signal [45]. One of the methods used for this purpose is to extract the Fast Fourier Transform (FFT) of the signal. FFT converts the signal from the time domain to the frequency domain. The formula of the FFT of the signal is demonstrated as

$$\mathbf{X}(\mathbf{f}) = \int x(t) * e^{-j2\pi ft} dt, \tag{5.5}$$

where $x(t)$ is the signal in time domain and the $X(f)$ is the signal in frequency domain [46, 47].

In order to determine whether the PCG signal contains abnormality, first of all, a database which was created to classify the heart sound signals [48], containing 1000 records with a length of 2 seconds, was examined and an algorithm was created from this data. In this database, heart sound signals which are taken from healthy people and also people with MVP, AS, MS and MR diseases, containing 200 records for each, are available in .wav format [48]. FFTs of the normal and the abnormal heart sound data were examined primarily to obtain the frequency domain information of the signal. Then, a relationship between the frequency components obtained for normal and abnormal HS is deduced. At this stage, it is expected that the dominant frequency for normal heart sound signals will be below 150 hz, so signals with a frequency component above 150 hz are considered to have high frequency components due to murmur. With the developed algorithm, First, the FFT is calculated to extract the frequency components of the signal. Then, the upper envelope curve is extracted on this FFT graph. The peak points and the frequency values corresponding to these peak points are located on this envelope graph. Among these amplitude values, the one with the maximum amplitude is determined and accepted as the dominant frequency of the

signal. After that, peaks with amplitude values that are less than 20 percent of the maximum amplitude value are eliminated from the peak array, since these peaks may occur due to noise or artifact in the signal. The frequency values of the remaining peaks are found in the array. The maximum frequency value is examined in the frequency values found. If this value is below 150 Hz, the signal is labeled as normal heart sound signal, because the normal heart sound signal is in the frequency range of 20 and 150 Hz. Otherwise, the signal is considered to contain murmurs with a higher frequency and it is labeled as abnormal heart sound.

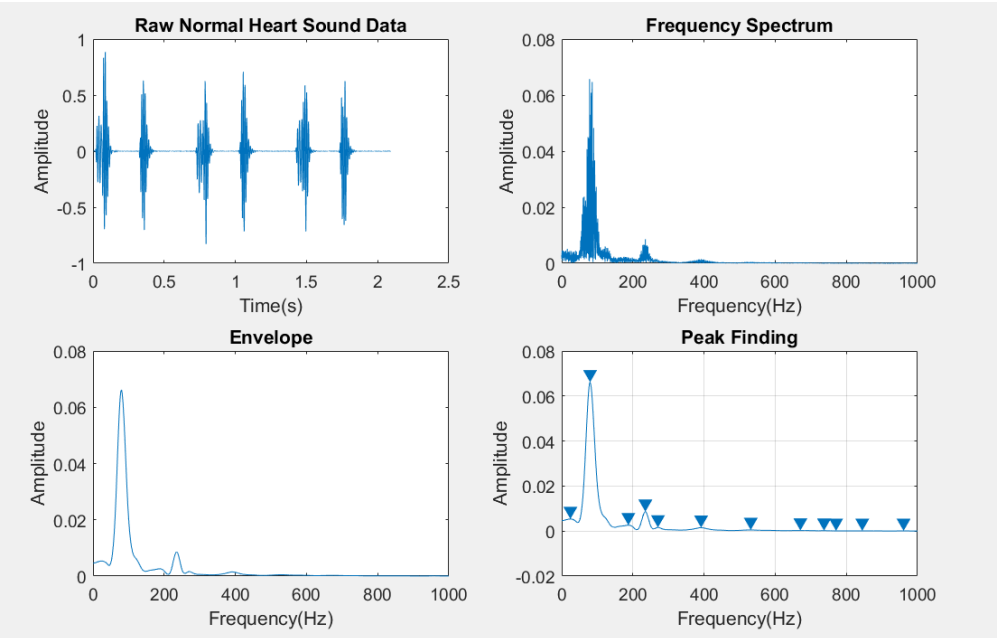

Figure 5.5. The Normal HS and FFT Analysis.

In Figure 5.5, normal heart sound data and its FFT analysis graphs are shown. The dominant frequency of the normal heart sound is found as 79.7 Hz which is below the 150 Hz threshold value determined by the algorithm. In aortic stenosis data which is shown in Figure 5.6, the maximum frequency component is found at 215.1 Hz, so it exceeds the determined threshold value. Thus, this data is labeled as abnormal. Similarly, in Figure 5.7, 5.8, and 5.9 maximum frequency values are found 163.1 Hz, 336.8 Hz, 363.5 Hz, respectively. Due to the fact that these values are greater than 150 Hz, these heart sound signals are labeled as abnormal.

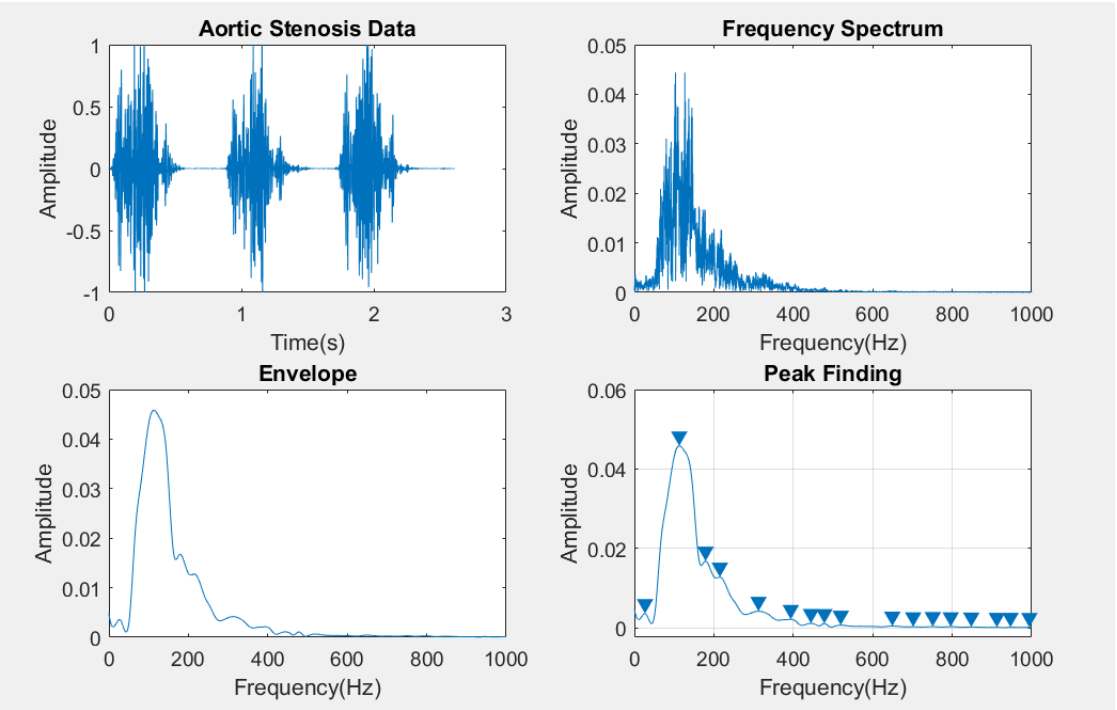

Figure 5.6. The Aortic Stenosis HS and FFT Analysis.

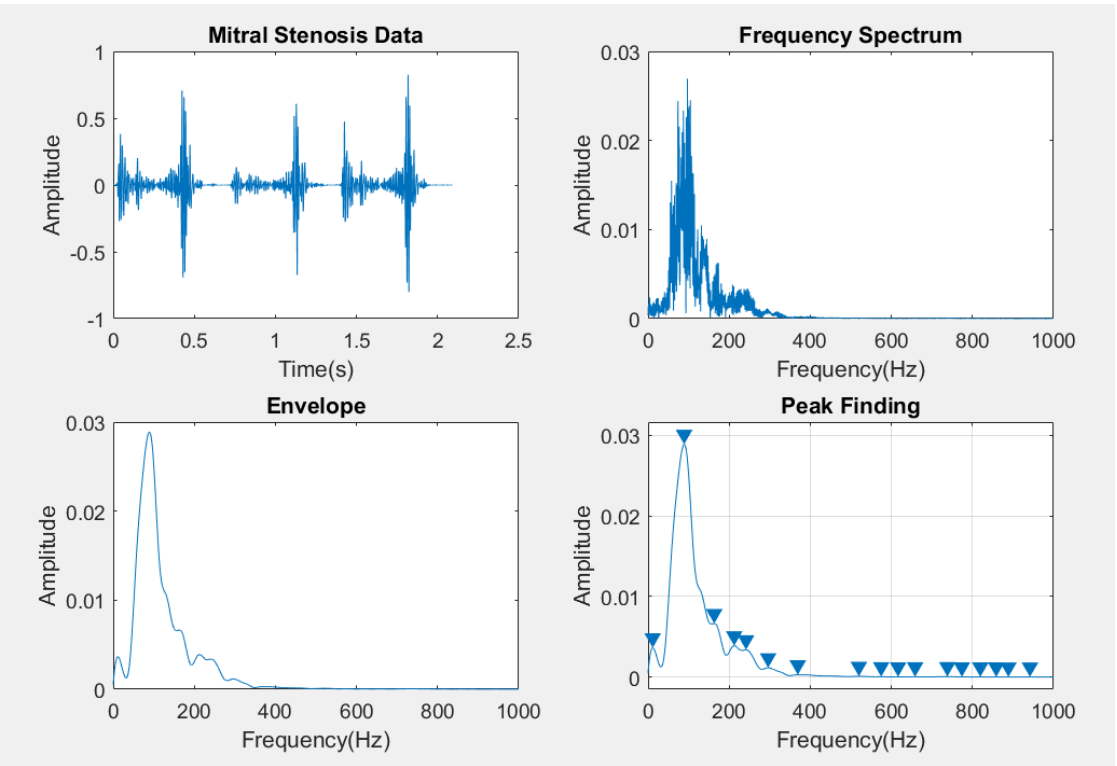

Figure 5.7. The Mitral Stenosis HS and FFT Analysis.

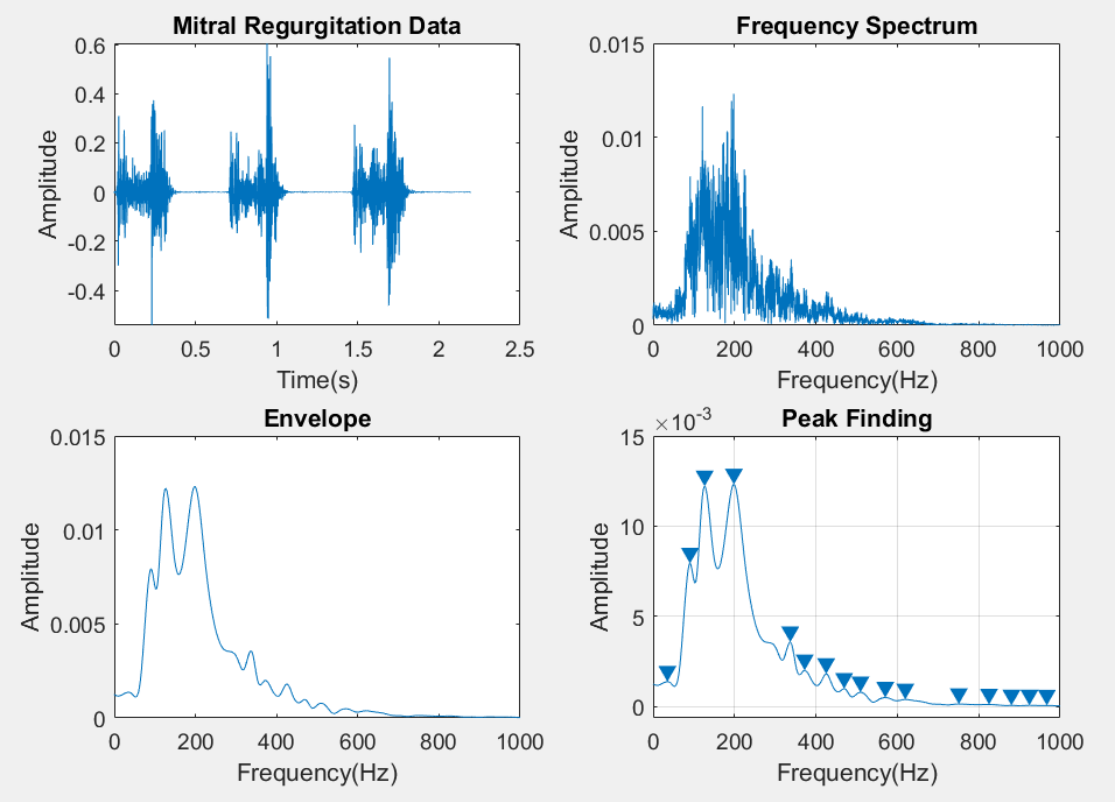

Figure 5.8. The Mitral Regurgitation HS and FFT Analysis.

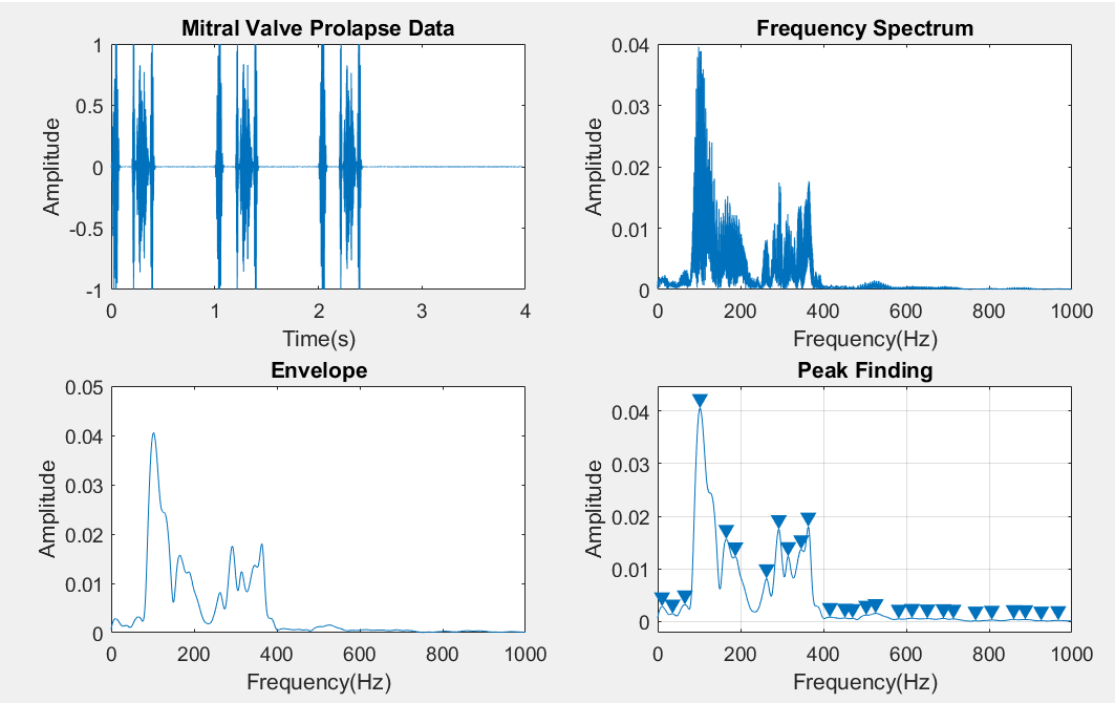

Figure 5.9. The Mitral Valve Prolapse HS and FFT Analysis.

Apart from the murmur sounds detected by the algorithm described above, S3 and S4 sounds which can be seen during the diastole period and have lower frequency indicate that the person may have heart disease. S3 sound is a component seen when there is a physical problem in the ventricle. It can occur when there is a sudden increase in the amount of blood pumped to the heart during diastole. It creates an abnormality in people over 40 years of age. On the other hand, the S4 sound is seen during the intense contraction of the atrium. And this sound component indicates that the person may have cardiac dysfunction [49].

Hilbert transform is one of the most frequently used analysis methods in the literature for the detection of abnormal heart sounds. With this method, it is possible to examine the heart sound in the time-frequency domain and extract the murmur sounds. In this analysis method, first of all, the signal is divided into intrinsic mode functions (IMFs). Empirical mode decomposition is used for this operation. Then, the Hilbert transforms of the obtained IMFs are extracted and thus instantaneous frequency and energy amplitude values can be examined [50].

This analysis was applied to the data labeled as the normal heart sound and the aortic stenosis heart sound in the database, and Hilbert transforms were examined in Figure 5.10 and Figure 5.11, respectively. All codes of the analysis system can be found in APPENDIX A.

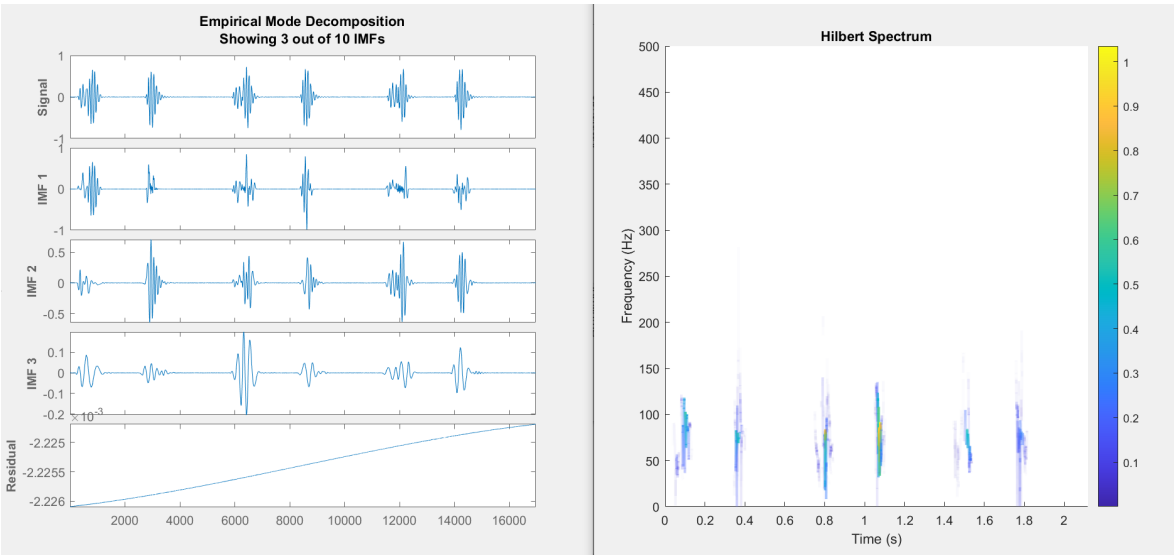

Figure 5.10. The IMFs and the Hilbert Transform of the Normal Heart Sound.

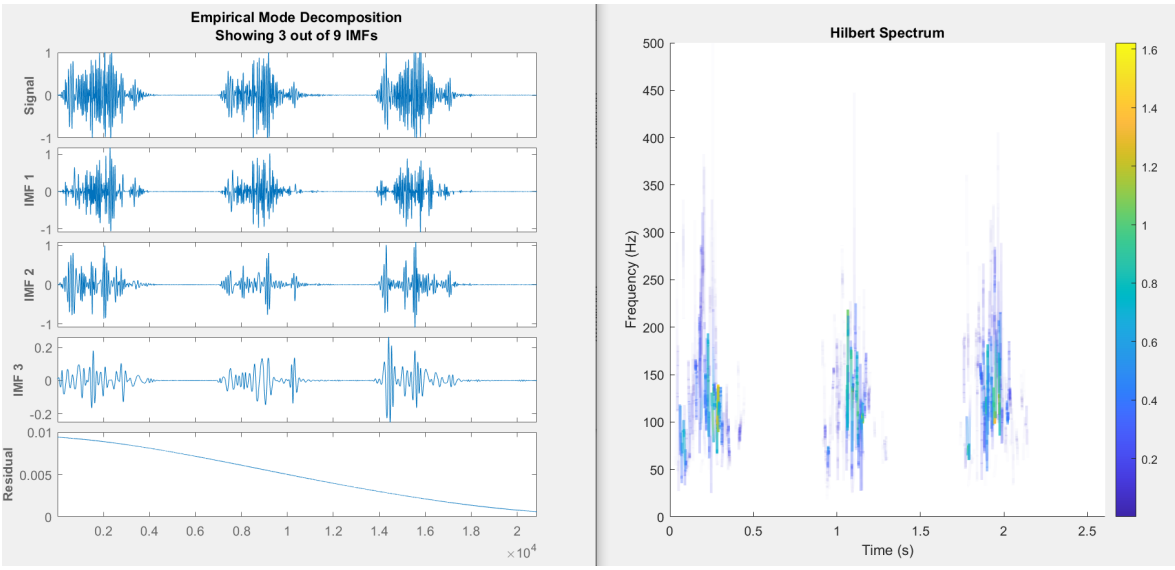

Figure 5.11. The IMFs and the Hilbert Transform of the Aortic Stenosis Murmurs.

5.3. Graphical User Interface

The user-friendly interface, designed in MATLAB R2021b for users to visually inspect and listen to heart sounds, includes information about the person who the recorded data belongs, raw data graphs and digitally filtered data graphs. At the same time, it allows the user to listen to the recorded heart sound at the desired volume

over the interface. Again, thanks to this interface, the users can see which parts of their bodies they should place the stethoscope head on to listen to the heart sound. In addition, the Shannon energy envelope of the signal and the extracted S1 and S2 peaks are visualized on the graphical interface for academic use. Heart rate and heart rate variability data are also displayed on the GUI, and the user can see whether the heart sound is abnormal or normal.

These graphs, heart sound and acquired results warn the people that there is a possibility that they have cardiac dysfunction and that they should seek the advice of a doctor. The designed application interface can be seen in the figures below. In Figure 5.12, raw data and its Shannon energy envelope are shown. Also, filtered data and S1 and S2 peaks can be seen in Figure 5.13.

Moreover, users can listen to the recorded heart sound for as long as they want after pressing the play button and can stop it whenever they want by using the stop button at the bottom left. The heart sound is best heard from the mitral area on the chest, so the user can check where the diaphragm should be placed from the top left view. At the same time, the user can listen to this sound with headphones over the sensor and determine the place where the sound is best received. Thanks to the designed interface, all signal processing processes have been automated and the user is able to access all information through a single interface.

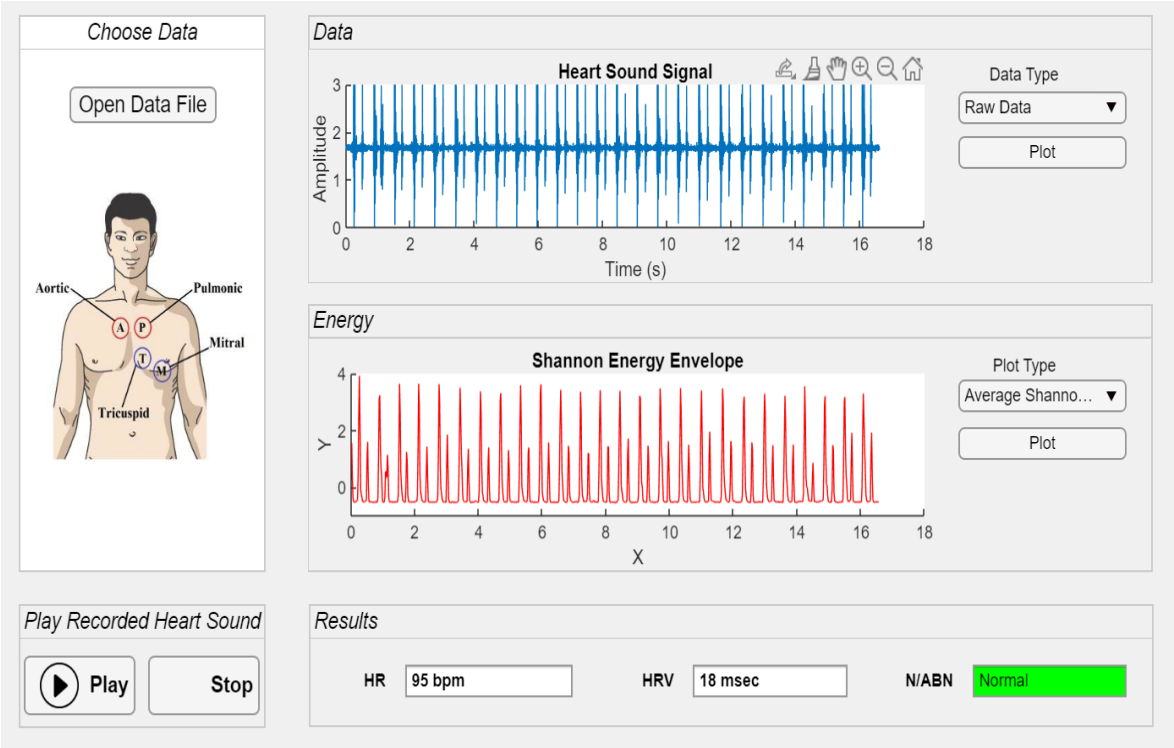

Figure 5.12. The GUI of the Heart Sound Analysis System.

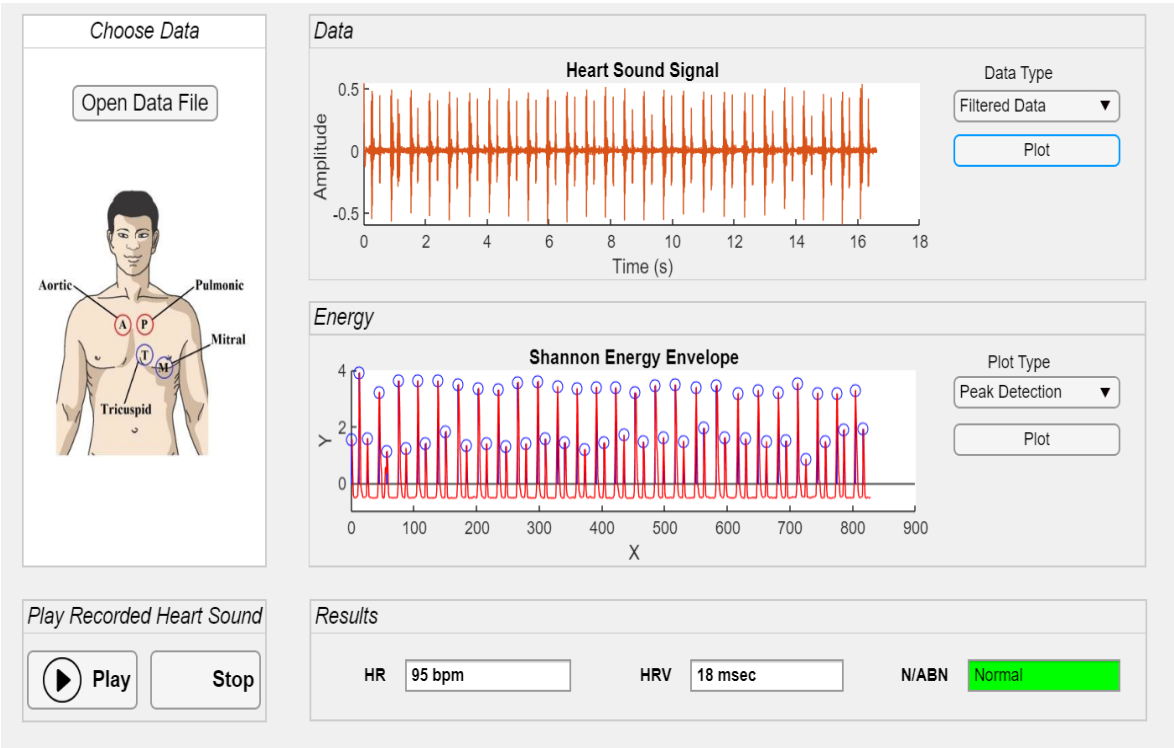

Figure 5.13. The Filtered Data and The Peak Detection Results on Designed GUI.

6. MECHANICAL STRUCTURE

6.1. Power Supply Unit

Low-cost Orion brand LIR 2032, 3.7 V rechargeable 20 mm and 2-legged lithium-ion battery is used for the power supply of the system. The supplies for the analog part and the digital part are separated, and 100 mA fuses are added to the supply paths to provide protection for both parts. Rechargeable batteries are used to supply the whole system. Also, these batteries can be charged via the charge circuit with the adaptor or micro USB. 230 V mains voltage is converted to 5 V with an adapter and connected to the input of the charging circuit. Small size TP4056 linear charging circuits with overcharge protection are used in this section. This circuit, which has a charging current of 1 A, also provides an adjustable charging current. For this process, it is sufficient to solder the resistors of suitable value on the charging circuit. The state of charge of the batteries can be observed via the indicator LEDs. During charging, the LED lights red. When charging is over, other LED lights blue [51].

In addition, there are 2 push buttons on the system, one of which is the on/off button of the system. The power is transferred to the analog part via this push button. This button is placed directly to the input of the TPS73633 integrated circuit. The circuit output is connected to the supply of the system via the designed PCB. In this way, all voltage values between 1.7 V and 5.5 V are converted to 3.3 V and transferred to the system. The other push-button is used to transfer power to the external supply input of the nRF 52 development kit and simultaneously connect the analog output of the PCB to the analog input pin of the nRF52 DK. For this part also, the battery supplies the nRF52 with 3.3 V over TPS73633. The components used in the power unit have been selected and designed to keep the cost of the sensor at a low level. The connection diagram of the power unit is depicted in Figure 6.1.

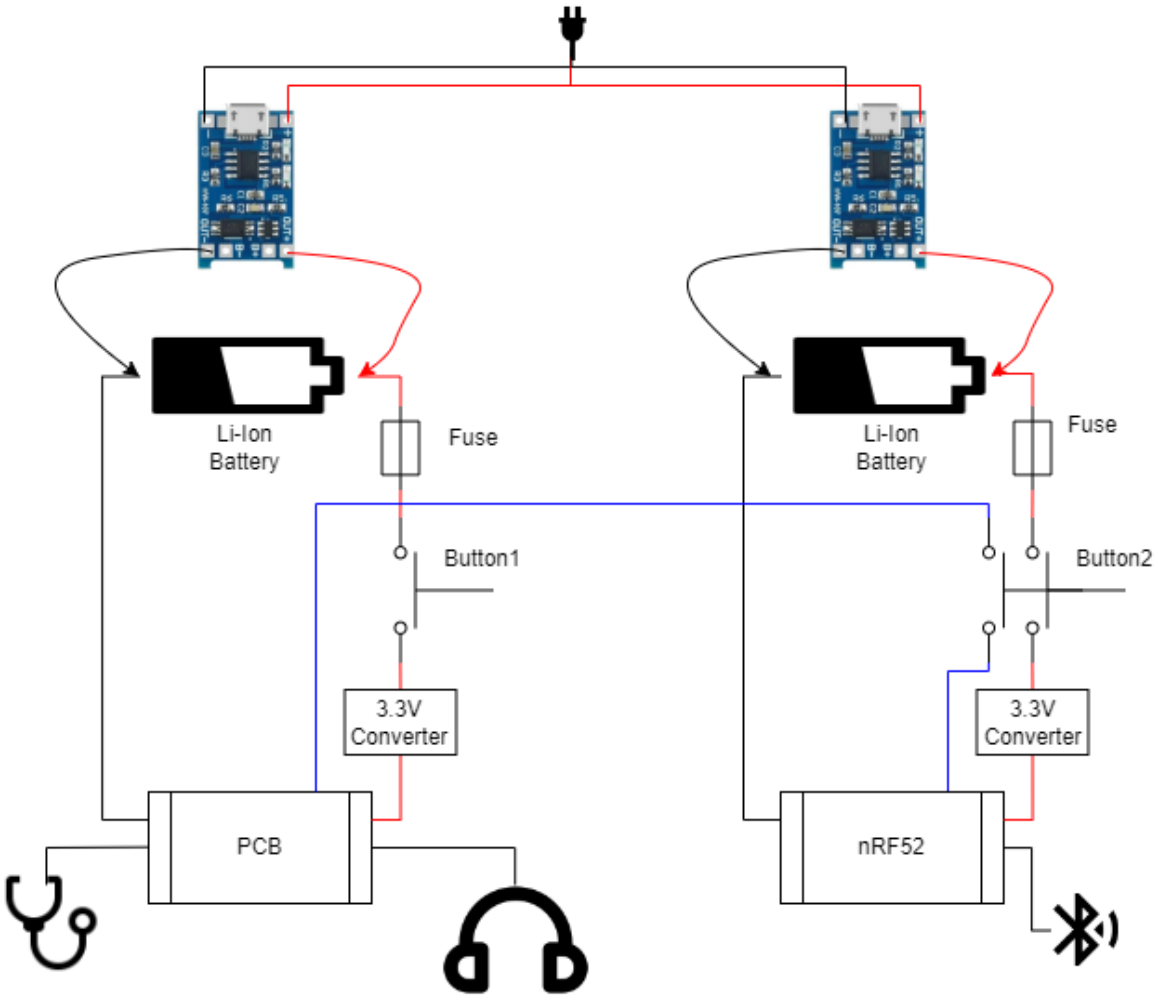

Figure 6.1. The Wiring Diagram.

6.2. 3D Printed Design

The heart sound recording and analysis device was designed and printed in 3D. For this process, fused deposition modeling (FDM) technology is used. In this way, the layers were fused in a single pattern and produced additively. In addition, care has been taken that the sensor is produced from an insulating material and that its cost is not too high. For this reason, Polylactic Acid (PLA) material was preferred for production. In order to preserve the portability of the device, its dimensions are designed as approximately 10 cm x 12 cm x 5 cm. There are 3 support columns to fix the development kit on the produced box floor. Apart from that, there are holes in with the appropriate sizes for microphone and headphone jack inputs, buttons and

charging port on the box. For ease of use, the power unit and the cover of the box are designed to be easily attached and removed with a channel system. 3D mechanical drawings are shown in the Figure 6.2, 6.3, 6.4. Also, the final views of the assembled box can be seen in Figure 6.5 and 6.6.

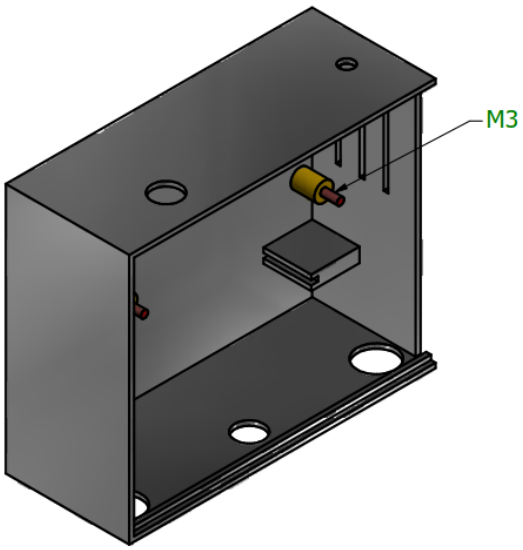

Figure 6.2. 3D Box Drawing.

Figure 6.3. The Top View of the 3D Box Drawing.

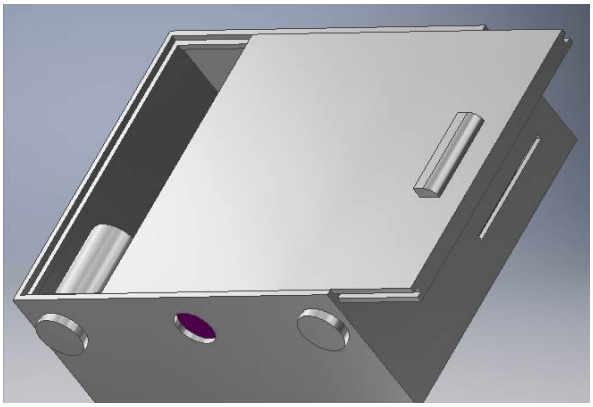

Figure 6.4. The Overall View of the 3D Box Drawing.

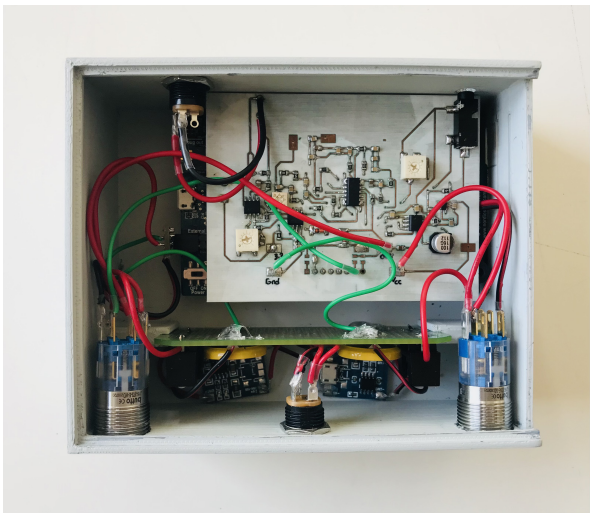

Figure 6.5. The Top View of the Box.

Figure 6.6. The Overall View of the Box.

7. RESULTS

As a result, after the system production is completed, heart sound recordings are taken from the volunteer participants. Participants are asked to put the diaphragm head on the right position on their chests while listening to heart sounds with headphones in a quiet environment during normal breathing. Heart rate values extracted from the heart sounds collected from healthy participants aged between 18-55 without time limitation are also compared with the HR value obtained with Xiaomi Mi Band. A few of the results acquired are shown in Figure 7.1, Figure 7.2, Figure 7.3, Figure 7.4, Figure 7.5. Also, algorithm results are shown in Table 7.1. Heart rate values are calculated with approximately ∓ 2.5 percent tolerance with respect to the Xiaomi Mi band. Apart from this, the accuracy rate of the algorithm which distinguishes normal and abnormal HS was checked by using randomly chosen 20 data for each class from the database [48]. Table 7.2 shows the results that are calculated as follows:

$$Accuracy\,(\%) = \frac{\#\ of\ Correct\ Predictions}{Total\ \#\ of\ Predictions} * 100. \tag{7.1}$$

Table 7.1. The Algorithm Results of the System.

Participant #	**Age / Gender**	**Heart Rate(bpm)**		**Health Condition**	**Algorithm Result**
		System	**Mi Band**		
1	27/Male	85	84	Healthy	N
2	29/Male	99	96	Healthy	N
3	26/Female	82	83	Healthy	N
4	29/Female	86	85	Healthy	N
5	24/Male	72	74	Healthy	N

Table 7.2. The Accuracy of the Algorithm.

Data Class	Normal	Abnormal	Accuracy (%)
N(20)	20	0	100
AS(20)	0	20	100
MS(20)	11	9	45
MR(20)	6	14	70
MVP(20)	10	10	50

According to these results, the algorithm can distinguish normal heart sound, aortic stenosis and mitral regurgitation with high accuracy. For the other 2 diseases, the algorithm accuracy of each class can be increased by setting different maximum frequency threshold values.

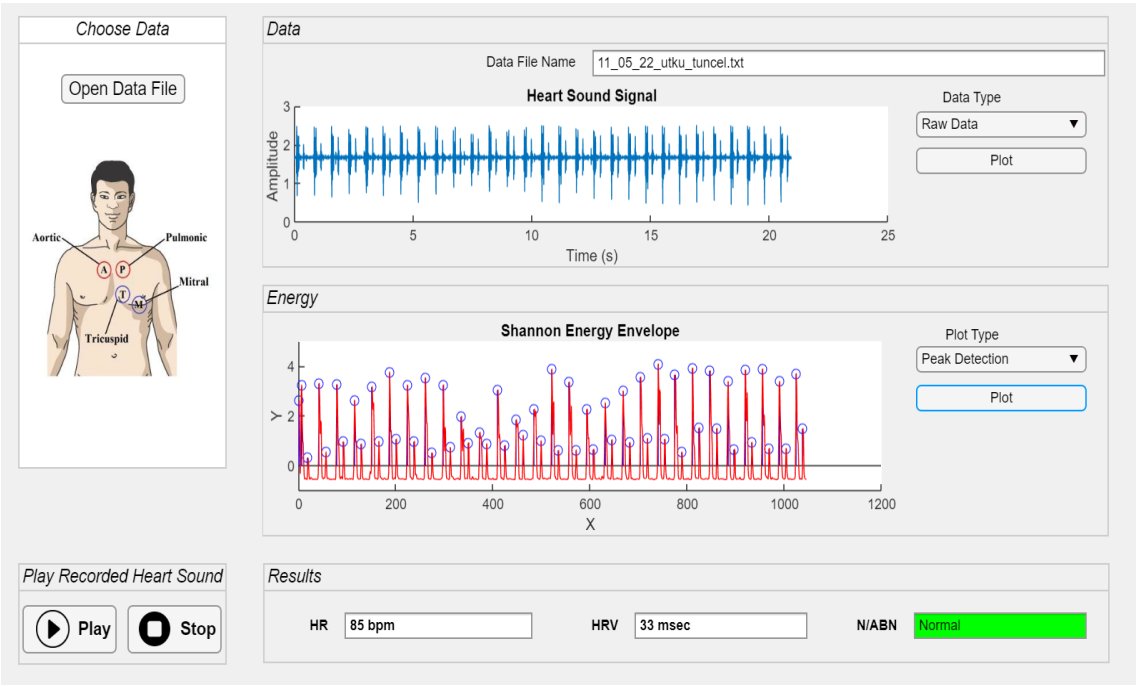

Figure 7.1. The System Results of Measurement1.

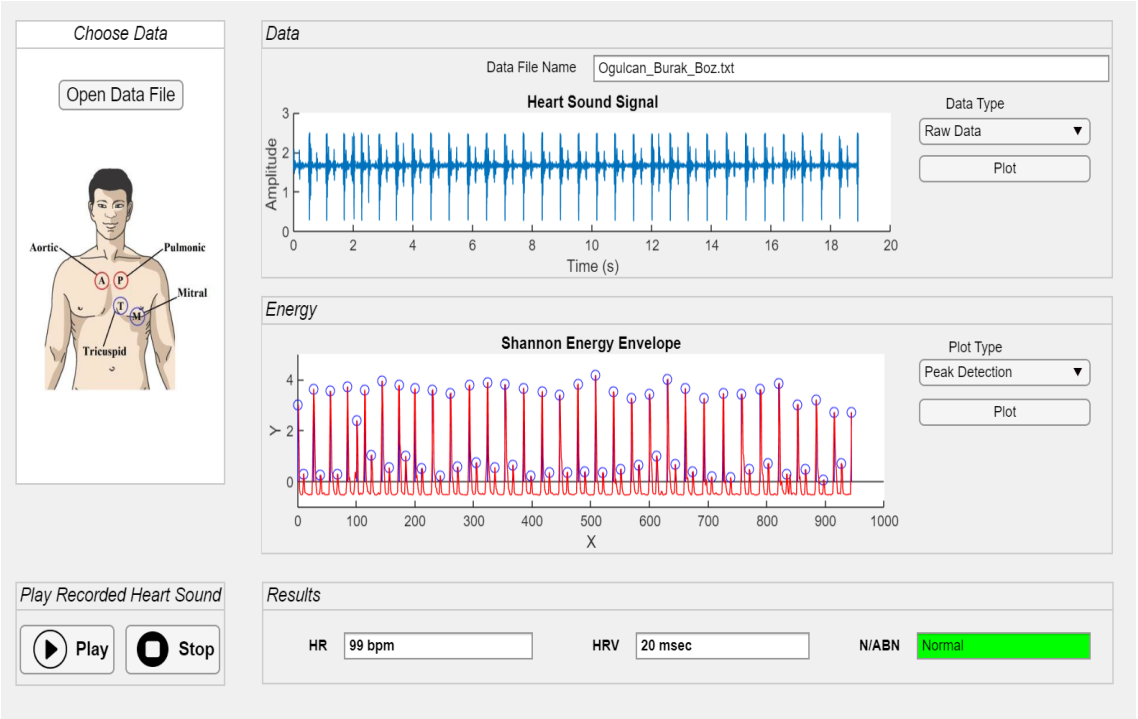

Figure 7.2. The System Results of Measurement2.

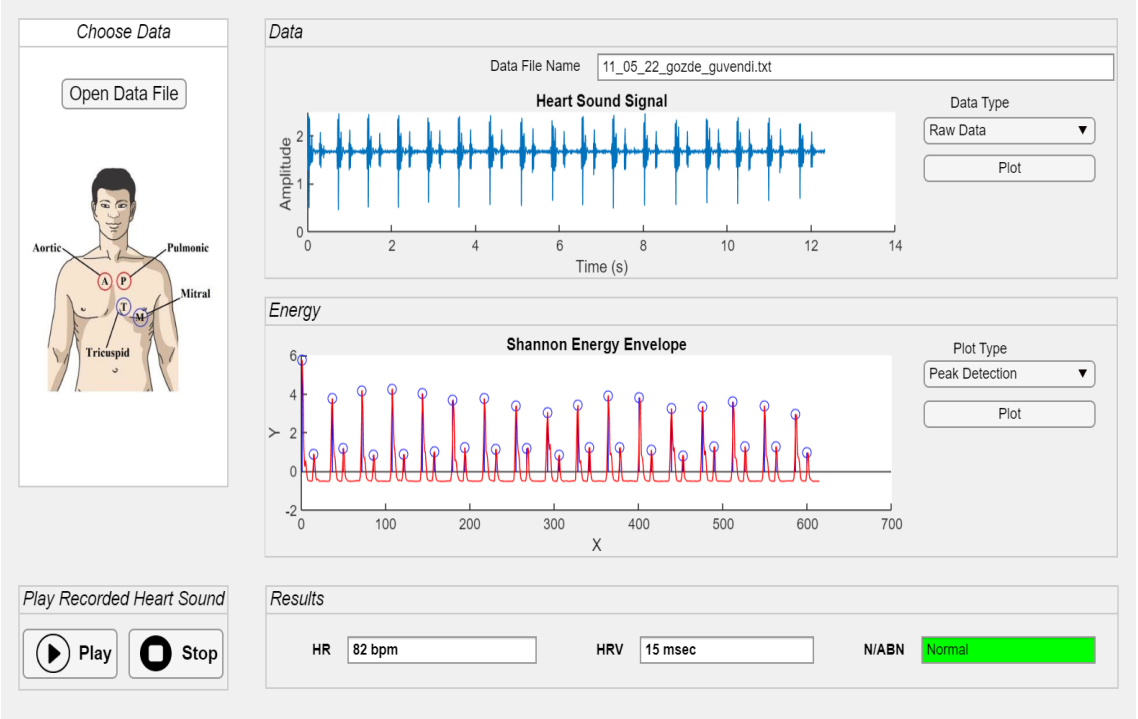

Figure 7.3. The System Results of Measurement3.

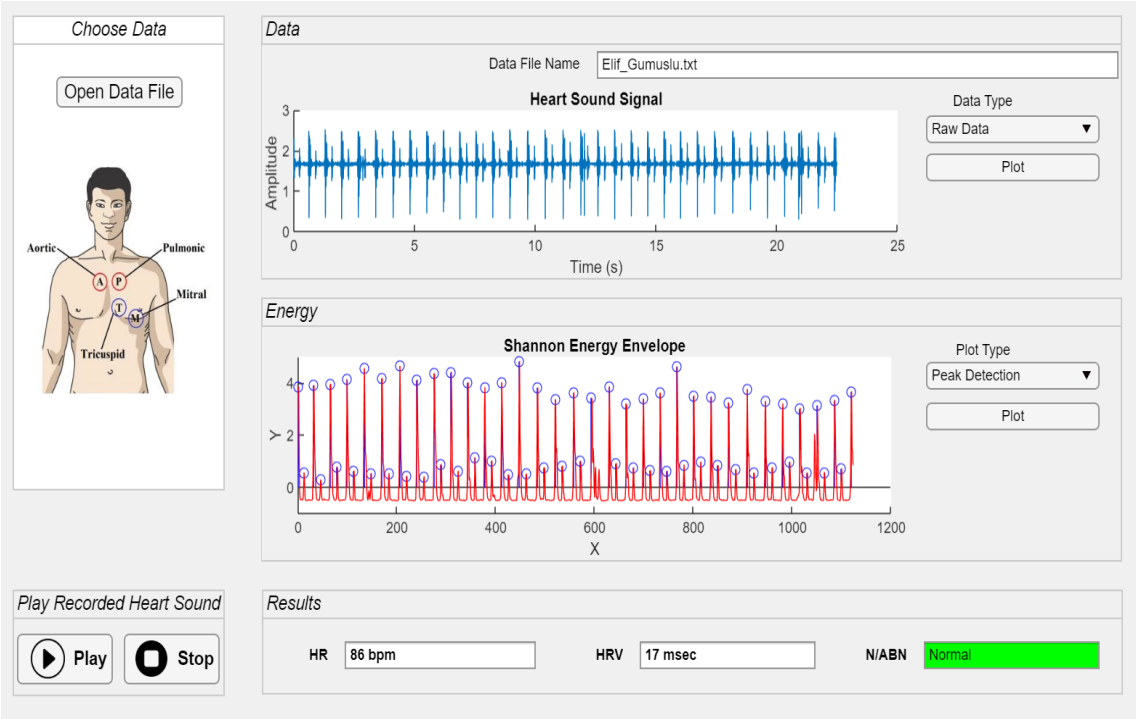

Figure 7.4. The System Results of Measurement4.

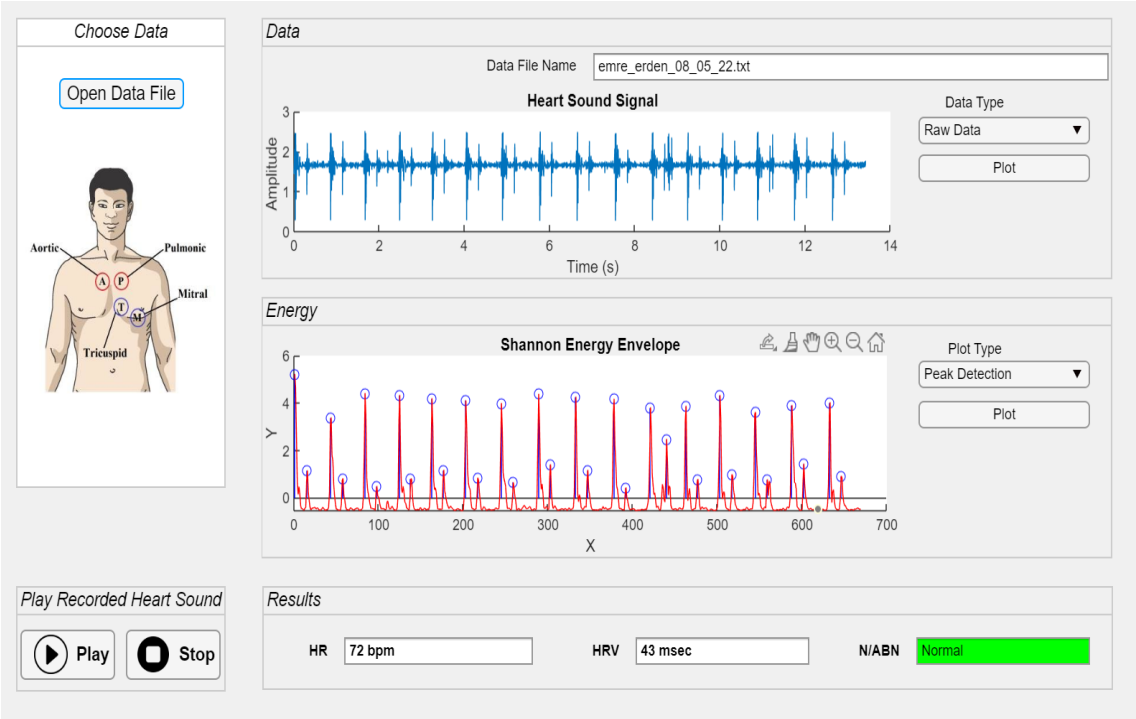

Figure 7.5. The System Results of Measurement5.

8. CONCLUSION

In conclusion, accurate analysis of heart sound for the detection of cardiovascular diseases with high mortality rates still maintains its importance today and researches on this subject are ongoing. This master thesis, which aims to contribute to these studies, includes electronic design, embedded system software, mechanical design, signal processing and interface development layers. The heart sound recording and analysis device has been designed, manufactured and tested completely. The heart sound signals of the participants, who participated in the experiment by filling out the ethics committee form, are examined with the device produced in accordance with the low power consumption and low-cost targets.

Furthermore, users can record the heart sounds for as long as they want and easily send this data to the computer via BLE and see the extracted results from the heart sounds on the designed interface. In signal processing stages, heart rate and heart rate variability data have been obtained by normalizing the heart sound and segmenting it. All these results are displayed in the designed user-friendly interface. In addition, the users can listen to heart sound recordings from the designed GUI as well as from the device directly. This study has been designed with a portable and easy-to-use device and an interface developed based on it, with the aim of providing convenience to users and healthcare professionals in the detection of cardiac dysfunction, and the accuracy of the outputs will be increased in the future studies.

Heart sound signal was acquired with different setups which were mentioned in the third section. Among these setups, the best result was obtained in the first setup in Figure 3.13 thanks to the acoustic stethoscope structure, since this structure is designed to obtain the heart sound without losses and contains specific parts such as eartips, eartube, tubing and diaphragm to prevent undesirable noises are heard. Thus, this setup transmits the heart sound to the electret microphone in the best way. However, the system uses an entire acoustic stethoscope to acquire the heart sounds and it disrupts the easy usability of the device. Therefore, heart sound was also

taken by other methods (setup2, setup3, and setup4 in Figure 3.13). In the system designed using a single-channel flexible tube (setup2), the noise effect was also more visible because the signal is transmitted to the microphone at a higher amplitude. On the other hand, in the system designed which was using a dual-channel tube and a microphone capsule (setup3 and setup4), the noise effect is less observed because the noise is transmitted to the microphone at a lower amplitude and then it can be filtered easily. Thus, the third and fourth setups were preferred for data acquisition, since they did not impair the usability of the device and peaks can be detected on the signal which was collected with these methods.

In addition to these setups, a piezoelectric sensor was also used to obtain a heart sound signal. The piezoelectric film sensor was placed in the diaphragm of the acoustic stethoscope and was expected to receive the vibration from the chest. However, as a result of the experiment, the desired vibration could not be accurately transmitted to the sensor surface, so the heart sound signal was distorted. This is due to the fact that mechanically the vibration could not be transmitted correctly to the piezo material using the diaphragm head. For this reason, a mechanical structure should be added to the design so as not to impair portability, and mechanical stress should be applied directly to the piezo material. An example of this mechanical structure is shown in some studies. These mechanical structures were not added to the designed system because they would increase the cost of the device.

In future work, classification feature can be added to the system by using machine learning or neural network algorithms such as a support vector machine with the database created by collecting data from people with aortic stenosis, mitral stenosis, mitral regurgitation and mitral valve prolapse diseases. Furthermore, the recorded medical data is transferred to a cloud system and can be used for telemedicine applications.

REFERENCES

1. WHO, *Cardiovascular Diseases (CVDs)*, 2021, `https://www.who.int/news-room/fact-sheets/detail/cardiovascular-diseases-(cvds)`, accessed on February 26, 2022.

2. Liu, C., D. Springer, Q. Li, B. Moody, R. Abad, F. Chorro, F. Castells Ramon, J. Roig, I. Silva, A. Johnson, Z. Syed, S. Schmidt, C. Papadaniil, L. Hadjileontiadis, H. Naseri, A. Moukadem, A. Dieterlen, C. Brandt, H. Tang and G. Clifford, "An Open Access Database for the Evaluation of Heart Sound Algorithms", *Physiological Measurement*, Vol. 37, No. 12, pp. 2181–2213, 2016.

3. Oktivasari, P., H. S. R. Amy, H. Freddy and Suprijadi, "Study and Analysis of Electronic Stethoscope Signal Using MATLAB & LabVIEW as Effective Tools", *Journal of Physics: Conference Series*, Vol. 1505, No. 1, p. 012054, 2020.

4. Varghees, V. N. and K. Ramachandran, "A Novel Heart Sound Activity Detection Framework for Automated Heart Sound Analysis", *Biomedical Signal Processing and Control*, Vol. 13, pp. 174–188, 2014.

5. Nishimura, R. A., C. M. Otto, R. O. Bonow, B. A. Carabello, J. P. r. Erwin, L. A. Fleisher, H. Jneid, M. J. Mack, C. J. McLeod, P. T. O'Gara, V. H. Rigolin, T. M. r. Sundt and A. Thompson, "AHA/ACC Focused Update of the 2014 AHA/ACC Guideline for the Management of Patients with Valvular Heart Disease: A Report of the American College of Cardiology/American Heart Association Task Force on Clinical Practice Guidelines", Vol. 135, pp. 1159–1195, 2017.

6. Nishimura, R. A., C. M. Otto, R. O. Bonow, B. A. Carabello, J. P. r. Erwin, R. A. Guyton, P. T. O'Gara, C. E. Ruiz, N. J. Skubas, P. Sorajja, T. M. r. Sundt and J. D. Thomas, "AHA/ACC Guideline for the Management of Patients With Valvular Heart Disease: executive summary: a report of the American College of Cardiology/American Heart Association Task Force on Practice Guidelines", Vol.

129, pp. 2440–2492, 2014.

7. Carabello, B. A. and F. A. J. Crawford, "Valvular Heart Disease", *The New England Journal of Medicine*, Vol. 337, pp. 32–41, 1997.

8. Leng, S., R. S. Tan, K. Chai, C. Wang, D. Ghista and L. Zhong, "The Electronic Stethoscope", *Biomedical Engineering Online*, Vol. 14, p. 66, 2015.

9. Knowles, A., *Regency Medicine - The Invention of the Stethoscope*, 2016, https://www.regencyhistory.net/2016/03/regency-medicine-invention-of.html, accessed on March 12, 2022.

10. Gupta, J. I. and M. J. Shea, *Cardiac Auscultation - Cardiovascular Disorders*, 2022, https://www.msdmanuals.com/professional/cardiovascular-disorders/approach-to-the-cardiac-patient/cardiac-auscultation#:~:text=Auscultation%20of%20the%20heart%20requires,the%20diaphragm%20of%20the%20stethoscope, accessed on May 03, 2022.

11. Ren, H., H. Jin, C. Chen, H. Ghayvat and W. Chen, "A Novel Cardiac Auscultation Monitoring System Based on Wireless Sensing for Healthcare", *IEEE Journal of Translational Engineering in Health and Medicine*, Vol. 6, pp. 1–12, 2018.

12. Writes, A., *The Stethoscope*, 2021, https://discover.hubpages.com/education/The-Stethoscope-, accessed on February 12, 2022.

13. MediLog-Bio-Health, *Parts of Stethoscope and Their Functions*, 2022, https://www.medilogbiohealth.com/2021/03/parts-of-stethoscope.html, accessed on April 08, 2022.

14. PUI Audio Inc., *POM-5242L-R*, 2010, https://eu.mouser.com/datasheet/2/334/POM-5242L-R-35293.pdf, accessed on January 03, 2022.

15. Kraman, S., G. Wodicka, Y. Oh and H. Pasterkamp, "Measurement of Respiratory

Acoustic Signals. Effect of Microphone Air Cavity Width, Shape, and Venting", *Chest*, Vol. 108, pp. 1004–1008, 1995.

16. Keim, R., *Understanding and Implementing Charge Amplifiers for Piezoelectric Sensor Systems - Technical Articles*, 2018, https://www.allaboutcircuits.com/technical-articles/understanding-and-implementing-charge-amplifiers-for-piezoelectric-sensor-s/, accessed on March 10, 2022.

17. Keim, R., *How to Design Charge Amplifiers for Piezoelectric Sensors*, 2018, https://www.allaboutcircuits.com/technical - articles/how - to - design - charge - amplifiers - piezoelectric - sensors/, accessed on March 10, 2022.

18. Texas Instruments, *Signal Conditioning Piezoelectric Sensors*, 2000, https://www.ti.com/lit/an/sloa033a/sloa033a.pdf, accessed on February 14, 2022.

19. TE Connectivity, *LDT0-28K LDT with Crimps Vibration Sensor/Switch*, 2017, https://eu.mouser.com/datasheet/2/418/5/NG_DS_LDT_with_Crimps_A1-1130083.pdf, accessed on November 30, 2021.

20. Measurement Specialties, *MiniSense 100 Vibration Sensor*, 2009, https://media.digikey.com/pdf/Data%20Sheets/Measurement%20Specialties%20PDFs/MiniSense_100.pdf, accessed on November 30, 2021.

21. Chen, H., S. Yu, H. Liu, J. Liu, Y. Xiao, D. Wu, X. Pan, C. Zhou, Y. Lei and S. Liu, "A Two-stage Amplified PZT Sensor for Monitoring Lung and Heart Sounds in Discharged Pneumonia Patients", *Microsystems & Nanoengineering*, Vol. 7, p. 55, 2021.

22. Zhang, S., R. Zhang, S. Chang, C. Liu and X. Sha, "A Low-Noise-Level Heart Sound System Based on Novel Thorax-Integration Head Design and Wavelet De-

noising Algorithm", *Micromachines*, Vol. 10, No. 12, p. 885, 2019.

23. Wang, T.-W. and S.-F. Lin, "Wearable Piezoelectric-Based System for Continuous Beat-to-Beat Blood Pressure Measurement", *Sensors*, Vol. 20, No. 3, p. 851, 2020.

24. Zhang, G., M. Liu, N. Guo and W. Zhang, "Design of the MEMS Piezoresistive Electronic Heart Sound Sensor", *Sensors*, Vol. 16, No. 11, p. 1728, 2016.

25. Microchip Technology Inc., *MCP6231/1R/1U/2/4 : 20 μA, 300 kHz Rail-to-Rail Op Amp*, 2020, `https://www.microchip.com/en-us/product/MCP6231`, accessed on January 14, 2022.

26. Wu, M. and G. Der-Khachadourian, "Digital Stethoscope A Portable, Electronic Auscultation Device", *Cornell University Electrical & Computer Engineering*.

27. Tang, Y., G. Cao, H. Li and K. Zhu, "The Design of Electronic Heart Sound Stethoscope Based on Bluetooth", *2010 4th International Conference on Bioinformatics and Biomedical Engineering*, pp. 1–4, 2010.

28. Chowdhury, M. E., A. Khandakar, K. Alzoubi, S. Mansoor, A. M. Tahir, M. B. I. Reaz and N. Al-Emadi, "Real-Time Smart-Digital Stethoscope System for Heart Diseases Monitoring", *Sensors*, Vol. 19, No. 12, p. 2781, 2019.

29. Microchip Technology Inc., *MCP601/1R/2/3/4 2.7V to 6.0V Single Supply CMOS Op Amps*, 2020, `https://ww1.microchip.com/downloads/en/DeviceDoc/21314g.pdf`, accessed on January 14, 2022.

30. Franco, S., *Design With Operational Amplifiers And Analog Integrated Circuits Fourth Edition*, McGraw-Hill Education, New York, 2014.

31. Texas Instruments, *TPS736xx Cap-Free, NMOS, 400-mA Low-Dropout Regulator with Reverse Current Protection*, 2015,

https://www.ti.com/lit/ds/symlink/tps736.pdf?ts=1651947224394, accessed on January 14, 2022.

32. Texas Instruments, *LM4875 750-mW, Stereo, Analog Input, Class-AB Audio Amplifier w/Precision DC Volume Control & Headphone Amplifier*, 2002, https://www.ti.com/lit/ds/symlink/lm4875.pdf?ts=1652212662316&ref_url=https%253A%252F%252Fwww.google.com%252F, accessed on January 14,2022.

33. Nordic Semiconductor, *nRF52832 Product Specification v1.4*, 2017, https://infocenter.nordicsemi.com/pdf/nRF52832_PS_v1.4.pdf, accessed on February 23, 2022.

34. Nordic Semiconductor, *nRF52832 Development Kit v1.1.x User Guide*, 2017, https://infocenter.nordicsemi.com/pdf/nRF52_DK_User_Guide_v1.2.pdf, accessed on February 23, 2022.

35. Nordic Semiconductor, *SAADC — Successive Approximation Analog-to-Digital Converter*, 2021, https://infocenter.nordicsemi.com/index.jsp?topic=%2Fstruct_nrf52%2Fstruct%2Fnrf52832_ps.html, accessed on March 14, 2022.

36. Nordic Semiconductor, *Exploring Different SAR ADC Analog Input Architectures*, 2021, https://www.analog.com/en/technical-articles/exploring-different-saradc-analog-input-architectures.html, accessed on March 14, 2022.

37. Baker, R. J., *CMOS: Circuit Design, Layout, and Simulation, 3rd Edition*, Wiley-IEEE Press, New York, 2011.

38. Nordic Semiconductor, *nRF52840 Dongle Product Brief*, https://www.nordicsemi.com/Products/Development-hardware/nrf52840-dongle, accessed on December 22, 2021.

39. Shi, W. Y., J. Mays and J.-C. Chiao, "Wireless Stethoscope for Recording Heart and Lung Sound", *2016 IEEE Topical Conference on Biomedical Wireless Technologies, Networks, and Sensing Systems (BioWireleSS)*, pp. 1–4, 2016.

40. Yu, F., A. Bilberg and F. Voss, "The Development of an Intelligent Electronic Stethoscope", *2008 IEEE/ASME International Conference on Mechtronic and Embedded Systems and Applications*, pp. 612–617, 2008.

41. Liang, H., S. Lukkarinen and I. Hartimo, "Heart Sound Segmentation Algorithm Based on Heart Sound Envelogram", *Computers in Cardiology 1997*, pp. 105–108, 1997.

42. Elite HRV, *Heart Rate Variability vs. Heart Rate*, 2021, `https://elitehrv.com/heart-rate-variability-vs-heart-rate`, accessed on April 14, 2022.

43. Shaffer, F., Z. M. Meehan and C. L. Zerr, "A Critical Review of Ultra-Short-Term Heart Rate Variability Norms Research", *Frontiers in Neuroscience*, Vol. 14, 2020.

44. Ortiz, R., R. González, M. Peña, S. Carrasco, M. Gaitán and C. Vargas, "Differences in Foetal Heart Rate Variability from Phonocardiography and Abdominal Electrocardiography", *Journal of Medical Engineering & Technology*, Vol. 26, No. 1, pp. 39–45, 2002.

45. Lubaib, P. and K. A. Muneer, "The Heart Defect Analysis Based on PCG Signals Using Pattern Recognition Techniques", *Procedia Technology*, Vol. 24, pp. 1024–1031, 2016.

46. Debbal, S. and F. Bereksi Reguig, "Frequency Analysis of the Heartbeat Sounds", *IJBSCHS*, Vol. 13, pp. 85–90, 2008.

47. Debbal, S., "Computerized Heart Sounds Analysis", *Discrete Wavelet Transforms*, chap. 5, IntechOpen, Rijeka, 2011.

48. Khan, Y., *Classification of Heart Sound Signal Using Multiple Features*, 2022, `https://github.com/yaseen21khan/Classification-of-Heart- Sound-Signal- Using- Multiple- Features- /blob/master/README.md`, accessed on March 18, 2022.

49. Li, S., F. Li, S. Tang and W. Xiong, "A Review of Computer-Aided Heart Sound Detection Techniques", *BioMed Research International*, Vol. 2020, pp. 1–10, 2020.

50. Tseng, Y. L., P. Y. Ko and F. S. Jaw, "Detection of the Third and Fourth Heart Sounds Using Hilbert-Huang Transform", *Biomedical Engineering Online*, Vol. 11, p. 8, 2012.

51. NanJing Top Power ASIC Corp., *TP4056 1A Standalone Linear Li-Ion Battery Charger with Thermal Regulation in SOP-8*, 2015, `https://rarecomponents.com/docs/TP4056.pdf`, accessed on February 02, 2022.

APPENDIX A: APPLICATION

```
% Button pushed function: OpenDataFileButton
function OpenDataFileButtonPushed(app, event)
global t;
global yw;
global val;
global Tp;
global P;
global c1;
global peakloc;
global Fs;

clear sound;

 [filename, pathname]=uigetfile('*.*','Choose Data File');
 myfilename=[pathname filename];
 file=readcell(myfilename);

 app.DataPanel.Visible='on';
 app.EnergyPanel.Visible='on';
 app.ResultsPanel.Visible='on';
 app.PlayRecordedHeartSoundPanel.Visible='on';
 app.NABNEditField.BackgroundColor='#FFFFFF';


 for i=1:size(file,1)
     data=file(i);
     if contains(data,"value (0x)")
         data=char(data);
         [startIndex,endIndex] = regexpi(data,"value");
```

```
          endIndex=endIndex(2)+7;
          data_=data(endIndex:end);
          data__{i}=data_;
      end
 end

idx = cellfun(@isempty,data__);
data___=data__(find(idx==0));


a=data___(1,4:length(data___)-2);
C = char(a);

Cx=C;

sdia=1;
for i=1:size(Cx,1)
    acnt=1;
    j=2;
    elem_cnt=0;
    while acnt<4
        if isequal(Cx(i,j),'3')
 elem_cnt=elem_cnt+1;
 if elem_cnt==1
     a=custom_convert(Cx(i,j+1));
 elseif elem_cnt==2
     b=custom_convert(Cx(i,j+1));
 elseif elem_cnt==3
     c=custom_convert(Cx(i,j+1));
 elseif elem_cnt==4
     d=custom_convert(Cx(i,j+1));
```

```
 end

        elseif Cx(i,j)=='0'
 acnt=acnt+1;
 if elem_cnt==1
     dummy_sum=a;
 elseif elem_cnt==2
     dummy_sum=a*10+b;
 elseif elem_cnt==3
     dummy_sum=a*100+b*10+c;
 elseif elem_cnt==4
     dummy_sum=a*1000+b*100+c*10+d;
 end
 gzd(sdia)=dummy_sum;
 sdia=sdia+1;
 elem_cnt=0;
 j=j+3;
        end

        j=j+3;


    end
end


num=transpose(gzd);
num=num*3.3/4096;
Fs=1250;
val= num(:,1);
L1=size(val,1);
```

```
t=(0:L1-1)/Fs;

valnorm1=(val)/max(abs(val));

% Filter Section

[B,A]=cheby1(2,0.2, [20 300]/(Fs/2), 'bandpass');
h1=dfilt.df2(B,A);
yw=filter(h1,valnorm1);

%Shannon envelope detection


N=length(yw);
windowRes=0.02;  %20ms
Ns=(Fs*windowRes);
Nw= floor((N/Ns));
i=1;
for c= 1:Nw
x=yw(i:i+Ns-1,1);
Es(c)= -1*(sum((x.^2) .* log (x.^2)))/(Ns);
i=i+Ns;
end
n=1;
for j=1:length(Es)
if j==length(Es), break, end
Es1(j)= sum(Es(n:n+1))/2;
n=n+1;
end
P= (Es1-mean(Es1,2))/std(Es1);
Tp=(1:size(Es1,2))*windowRes;
```

```
th=floor(max(P))*0.1;
peakmeannew=0;
peakmeanold=10;
thcount=0;
thcountif=0;

while abs(peakmeanold-peakmeannew) > 1


% Peak finder
[peakloc,peakval]=peakfinder(P,(max(P)-min(P))/6, th,1);


%heartrate intervals calculation

I=1;
K=1;
L=1;
ssys=0;
sdia=0;
%J=1;
for I=1:(numel(peakloc))-1
J(I)=peakloc(I+1)-peakloc(I);
end
peakmeanold = peakmeannew;
peakmeannew = mean(J);


if abs(peakmeanold-peakmeannew) > 1
```

```
    th=th-0.2;
%     thcountif=thcountif+1;
end
% thcount=thcount+1;
end


Dp=diff(peakloc);
funsum= @(x) sum (x);
Dnew= blkproc (Dp, [1 2],funsum);
Fr=find (Dnew>=55 & Dnew<=120);
DelN=Dnew (Fr).* windowRes * Fs ;
%heartRate= mean(60*Fs./DelN);

%systolics
for I=1:numel(J)
if J(I)< mean(J)
ssys(K)=J(I);
K=K+1;
end
end

%diastolics
for I=1:numel(J)
if J(I)> mean(J)
sdia(L)=J(I);
L=L+1;
end
end

ssysT=ssys*windowRes;
```

```
sysmean=mean(ssysT);
sdiaT=sdia*windowRes;
diamean=mean(sdiaT);

ssys1=ssys;
meansys=mean(ssys1);
stdsys=std(ssys1);
gg=1;
delpeak=0;
for I=1:numel(ssys1);
while isnan(ssys1(I));
I=I+1;
end
if ssys1(I)<floor(meansys-stdsys)-2||...
ssys1(I)>ceil(meansys+stdsys)+2;
    delpeak(gg)=ssys1(I);
    gg=gg+1;
    ssys1(I) = NaN;
end
end
ssys2 = ssys1(~isnan(ssys1));

sdia1=sdia;
meandia=mean(sdia1);
stddia=std(sdia1);
for I=1:numel(sdia1)
while isnan(sdia1(I))
I=I+1;
end
if sdia1(I) < floor(meandia - stddia)-2
    delpeak(gg)=sdia1(I);
```

```
    gg=gg+1;
sdia1(I) = NaN;
end
end
sdia2 = sdia1(~isnan(sdia1));

hrt=(mean(ssys2)+mean(sdia2))*windowRes;
hr=60/hrt;

c1=peakval;
for i=2:length(peakloc);
    count=peakloc(i)-peakloc(i-1);
    for dp=1:length(delpeak)
        if count==delpeak(dp)
 if peakval(i)>peakval(i-1)
     c1(i-1) = NaN;
 else
     c1(i)= NaN;
 end
        end
    end
end


switch app.DataTypeDropDown.Value
 case 'Raw Data'
     hold(app.UIAxes,'off');
     plot (app.UIAxes,t,val);
 case 'Filtered Data'
     hold(app.UIAxes,'off');
     plot (app.UIAxes,t,yw);
```

```
end

switch app.PlotTypeDropDown.Value
    case 'Average Shannon Energy Envelope'
     hold(app.UIAxes_2,'off');
     plot (app.UIAxes_2,Tp,P,'r');

 case 'Peak Detection'
     hold(app.UIAxes_2,'off');
    stem(app.UIAxes_2,peakloc, c1,'b','Marker', 'o');
    hold(app.UIAxes_2,'on');
    plot (app.UIAxes_2,P,'r');
end

app.HREditField.Value = sprintf('%.0f bpm',hr);

%HRV Calculation
hcsize=min([length(sdia2) length(ssys2)]);
HC=sdia2(1,1:hcsize)+ssys2(1,1:hcsize);
%systole + diastole = heart cycle

for i=1:hcsize-1

    Vr(1,i)=abs(HC(1,i+1)-HC(1,i));

end

HRV=mean(Vr)*windowRes*1000; %in ms

app.HRVEditField.Value = sprintf('%.0f msec',HRV);
```

```
app.DataFileNameEditField.Value = sprintf('%s',filename);

%Normal Abnormal
FFT = fft(yw);
P2 = abs(FFT/L1);
P1 = P2(1:L1/2+1);
P1(2:end-1) = 2*P1(2:end-1);
fff = Fs*(0:(L1/2))/L1;

[Envhigh,Envlow]=envelope(P1,30,'peak');
[pks,locs]=findpeaks(Envhigh,fff);

pksmax=max(pks);
locsfind=locs;
 for pkscount= 1:length(pks)
     if pks(pkscount)<(pksmax*0.2)
         locsfind(pkscount)=NaN;
     end
 end
locsfind = locsfind(~isnan(locsfind));
locsmax=max(locsfind);

if locsmax < 150
    app.NABNEditField.Value = sprintf('Normal');
    app.NABNEditField.BackgroundColor='#00FF00';
else
    app.NABNEditField.Value = sprintf('Abnormal');
    app.NABNEditField.BackgroundColor='#FF0000';
end
```

```
function inte=custom_convert(sayi)
if sayi=='0'
    inte=0;
elseif sayi == '1'
    inte=1;
elseif sayi == '2'
    inte=2;
elseif sayi == '3'
    inte=3;
elseif sayi == '4'
    inte=4;
elseif sayi == '5'
    inte=5;
elseif sayi == '6'
    inte=6;
elseif sayi == '7'
    inte=7;
elseif sayi == '8'
    inte=8;
elseif sayi == '9'
    inte=9;
elseif sayi=='D'
    inte=NaN;
elseif sayi=='A'
    inte=NaN;
end
end

function varargout = peakfinder(x0, sel, thresh, extrema,...
includeEndpoints, interpolate)
```

```
narginchk(1, 6);
nargoutchk(0, 2);
s = size(x0);
flipData =  s(1) < s(2);
len0 = numel(x0);
if len0 ~= s(1) && len0 ~= s(2)
    error('PEAKFINDER:Input','The input data must be a vector')
elseif isempty(x0)
    varargout = {[],[]};
    return;
end
if ~isreal(x0)
    warning('PEAKFINDER:NotReal','Absolute value of data...
    will be used')
    x0 = abs(x0);
end
if nargin < 2 || isempty(sel)
    sel = (max(x0)-min(x0))/4;
elseif ~isnumeric(sel) || ~isreal(sel)
    sel = (max(x0)-min(x0))/4;
    warning('PEAKFINDER:InvalidSel',...
        'The selectivity must be a real scalar...
        A selectivity of %.4g will be used',sel)
elseif numel(sel) > 1
    warning('PEAKFINDER:InvalidSel',...
        'The selectivity must be a scalar. ...
        The first selectivity value in the vector will be used.')
    sel = sel(1);
end
if nargin < 3 || isempty(thresh)
```

```
    thresh = [];
elseif ~isnumeric(thresh) || ~isreal(thresh)
    thresh = [];
    warning('PEAKFINDER:InvalidThreshold',...
        'The threshold must be a real scalar...
        No threshold will be used.')
elseif numel(thresh) > 1
    thresh = thresh(1);
    warning('PEAKFINDER:InvalidThreshold',...
        'The threshold must be a scalar.  The first threshold...
        value in the vector will be used.')
end
if nargin < 4 || isempty(extrema)
    extrema = 1;
else
    extrema = sign(extrema(1));
    if extrema == 0
        error('PEAKFINDER:ZeroMaxima','Either 1 (for maxima) or...
        -1 (for minima) must be input for extrema');
    end
end
if nargin < 5 || isempty(includeEndpoints)
    includeEndpoints = true;
end
if nargin < 6 || isempty(interpolate)
    interpolate = false;
end
x0 = extrema*x0(:);
thresh = thresh*extrema;
dx0 = diff(x0);
dx0(dx0 == 0) = -eps;
```

```
ind = find(dx0(1:end-1).*dx0(2:end) < 0)+1;
if includeEndpoints
    x = [x0(1);x0(ind);x0(end)];
    ind = [1;ind;len0];
    minMag = min(x);
    leftMin = minMag;
else
    x = x0(ind);
    minMag = min(x);
    leftMin = min(x(1), x0(1));
end
% x only has the peaks, valleys, and possibly endpoints
len = numel(x);
if len > 2
    tempMag = minMag;
    foundPeak = false;
    if includeEndpoints
        signDx = sign(diff(x(1:3)));
        if signDx(1) <= 0
 if signDx(1) == signDx(2)
     x(2) = [];
     ind(2) = [];
     len = len-1;
 end
        else
 if signDx(1) == signDx(2)
     x(1) = [];
     ind(1) = [];
     len = len-1;
 end
        end
```

```
    end
    if x(1) >= x(2)
        ii = 0;
    else
        ii = 1;
    end

    maxPeaks = ceil(len/2);
    peakLoc = zeros(maxPeaks,1);
    peakMag = zeros(maxPeaks,1);
    cInd = 1;

    while ii < len
        ii = ii+1; % This is a peak

        if foundPeak
tempMag = minMag;
foundPeak = false;
        end

        if x(ii) > tempMag && x(ii) > leftMin + sel
tempLoc = ii;
tempMag = x(ii);
        end

        if ii == len
break;
        end
        ii = ii+1;

        if ~foundPeak && tempMag > sel + x(ii)
```

```
foundPeak = true;
leftMin = x(ii);
peakLoc(cInd) = tempLoc;
peakMag(cInd) = tempMag;
cInd = cInd+1;
       elseif x(ii) < leftMin
leftMin = x(ii);
       end
   end

   if includeEndpoints
       if x(end) > tempMag && x(end) > leftMin + sel
peakLoc(cInd) = len;
peakMag(cInd) = x(end);
cInd = cInd + 1;
       elseif ~foundPeak && tempMag > minMag
peakLoc(cInd) = tempLoc;
peakMag(cInd) = tempMag;
cInd = cInd + 1;
       end
   elseif ~foundPeak
       if x(end) > tempMag && x(end) > leftMin + sel
peakLoc(cInd) = len;
peakMag(cInd) = x(end);
cInd = cInd + 1;
       elseif tempMag > min(x0(end), x(end)) + sel
peakLoc(cInd) = tempLoc;
peakMag(cInd) = tempMag;
cInd = cInd + 1;
       end
   end
```

```
    if cInd > 1
        peakInds = ind(peakLoc(1:cInd-1));
        peakMags = peakMag(1:cInd-1);
    else
        peakInds = [];
        peakMags = [];
    end
else
    [peakMags,xInd] = max(x);
    if includeEndpoints && peakMags > minMag + sel
        peakInds = ind(xInd);
    else
        peakMags = [];
        peakInds = [];
    end
end

if ~isempty(thresh)
    m = peakMags>thresh;
    peakInds = peakInds(m);
    peakMags = peakMags(m);
end
if interpolate && ~isempty(peakMags)
    middleMask = (peakInds > 1) & (peakInds < len0);
    noEnds = peakInds(middleMask);
    magDiff = x0(noEnds + 1) - x0(noEnds - 1);
    magSum = x0(noEnds - 1) + x0(noEnds + 1)  - 2 * x0(noEnds);
    magRatio = magDiff ./ magSum;
    peakInds(middleMask) =peakInds(middleMask)-magRatio/2;
    peakMags(middleMask) =peakMags(middleMask)-magRatio.*magDiff/8;
```

```
end

if flipData
    peakMags = peakMags.';
    peakInds = peakInds.';
end

if extrema < 0
    peakMags = -peakMags;
    x0 = -x0;
end

if nargout == 0
    if isempty(peakInds)
        disp('No significant peaks found')
    else
        figure;
        plot(1:len0,x0,'.-',peakInds,peakMags,'ro','linewidth',2);
    end
else
    varargout = {peakInds,peakMags};
end

end
        end

% Button pushed function: PlotButton
function PlotButtonPushed(app, event)
       global t;
       global val;
       global yw;
```

```
        switch app.DataTypeDropDown.Value
 case 'Raw Data'
     hold(app.UIAxes,'off');
     plot (app.UIAxes,t,val);
 case 'Filtered Data'
     hold(app.UIAxes,'off');
     plot (app.UIAxes,t,yw,'Color',[0.8500 0.3250 0.0980]);

        end
        end

% Button pushed function: PlotButton_2
function PlotButton_2Pushed(app, event)
 global Tp;
 global P;
 global c1;
 global peakloc;

        switch app.PlotTypeDropDown.Value
 case 'Average Shannon Energy Envelope'
     hold(app.UIAxes_2,'off');
     plot (app.UIAxes_2,Tp,P,'r');
 case 'Peak Detection'
     hold(app.UIAxes_2,'off');
    stem(app.UIAxes_2,peakloc, c1,'b','Marker', 'o');
    hold(app.UIAxes_2,'on');
    plot (app.UIAxes_2,P,'r');
        end
        end
```

```
% Button pushed function: PlayButton
function PlayButtonPushed(app, event)
 global yw;
 global Fs;

 sound(yw,Fs);
        end

% Button pushed function: StopButton
function StopButtonPushed(app, event)
 clear sound;
        end
    end
```